A Two-Dimensional Model of Plasma Transport and Chemistry in the Jovian Magnetosphere

Ron Schreier[1] and Aharon Eviatar[2]
Department of Geophysics and Planetary Sciences, The Raymond and Beverly Sackler Faculty of Exact Sciences, Tel Aviv University, Ramat Aviv, Israel.

Vytenis M. Vasyliūnas
Max–Planck–Institut für Aeronomie, Katlenburg–Lindau, Germany.

Received ____________________; accepted ____________________

For submission to JGR -January 25, 1998

Short title: PLASMA TRANSPORT IN THE IO TORUS.

---

[1]Based on a dissertation submitted to Tel Aviv University in partial fulfillment of the requirements for the degree of Doctor of Philosophy

[2]On sabbatical leave 1996-97 at The Johns Hopkins University, Applied Physics Laboratory, Laurel MD, USA

Abstract.

A 2-D model of plasma transport and chemistry in the Jovian inner magnetosphere that enables us to calculate ion and electron densities and temperatures as well as their radiative emission properties is presented. As input data the model uses (assumed) neutral densities, arbitrary initial ion densities, and ion and electron (both thermal and hot) temperatures given by the published empirical model derived from Voyager data. Six thermal ion species, three hot ion species, and both thermal and hot electrons are included. The calculated ion partitioning is similar to the results of previous numerical models (rather than the empirical model). The observed general increase in temperature of both the ions and electrons vs. distance can be accounted for by a distributed neutral source. Model electron temperature (and thus torus emission) was found to be less than expected. Of three proposed mechanisms that might account for the observed electron heating, namely, (a) an increase in the temperature of the thermal ions, resulting in electron heating via Coulomb collisions, (b) hot ions, presumably of ring current origin, diffusing inwards and heating the thermal electrons, and (c) a flux of suprathermal electrons, alternative (b) is most strongly supported by our model.

Introduction

The standard theoretical model of the Io plasma torus, generally referred to as neutral cloud theory [*Barbosa et al.*, 1983; *Smith and Strobel*, 1985; *Barbosa*, 1994] claims to account successfully for most of the observed properties of the torus. The ion source for the torus is electron impact ionization of neutral gas atoms that escape from Io and form a neutral cloud. The energy source for the EUV emission is the rotation of Jupiter, by means of the so-called pickup energy associated with the assimilation of the new ions in the plasma corotating with Jupiter. The ions are cooled by Coulomb collisions with electrons, and the electrons are then cooled by radiative losses. The electron temperature is fixed at a value corresponding to the energy balance between ion-electron Coulomb collisions and the plasma radiative loss function.

In spite of the apparent success of neutral cloud theory, there is an opposing school; the so-called "energy crisis" evoked by *Shemansky* [1988] who doubted the ability of the neutral cloud theory to explain the high torus emission He found that it can account for $\sim 1/3$ of the total emission required to maintain the torus. Observations of the plasma torus using ground-based, Earth satellite, and spacecraft instruments have uniformly indicated an average partitioning of sulfur ions $[S^+]/[S^{++}] < 1$ [*Moos et al.*, 1985] that is indicative of a high electron temperature. Because neutral cloud theory can only support a dominantly singly ionized system, it was argued by *Smith et al.* [1988] that a large fraction of the energy required to account for the Io torus must be supplied by non-local energy input.

Many issues in the physics of the Io torus in the Jovian magnetosphere remain unresolved. One of the outstanding issues is the mechanism of outward transport of iogenic plasma. *Siscoe et al.* [1981] noted that the pressure gradient of the hot plasma can suppress or enhance the interchange transport, according to the direction of the pressure gradient. The "ramp" region was pointed out as an indicator for a pressure gradient suppression of the outward transport of plasma torus.

Previous models[*Barbosa et al.*, 1983; *Smith and Strobel*, 1985; *Shemansky*, 1988; *Barbosa*, 1994] dealt with the chemistry of the torus but had at most a one-dimensional treatment of transport. *Richardson* [1992] had a two-dimensional transport but no chemistry. We present results obtained from a numerical model including both chemistry and two-dimensional plasma transport of the Io torus. We first first summarize plasma processes in the torus incorporated in the model and then present the model itself. Using as input the neutral sulfur and oxygen densities and plasma sources, we obtain the diffusion coefficient, plasma densities and temperatures. We then compare the calculated results with observations [*Bagenal and Sullivan*, 1981; *Bagenal*, 1994] and discuss several mechanisms which might explain the discrepancies.

Description

The diffusion equation generally used is a radial Fokker-Planck equation with transport terms and loss terms that are independent of each other [*Dungey*, 1965]

$$\frac{\partial n^*}{\partial t} = \frac{\partial}{\partial r}\left[\frac{D}{r^2}\frac{\partial(r^2 n^*)}{\partial r}\right] + \mathcal{S} - \mathcal{L}. \qquad (1)$$

Here n^* is any quantity contained in a flux tube as it moves under the interchange motion, r is the radial distance, D is the diffusion coefficient, and $\mathcal{S}$ and $\mathcal{L}$ are the source and loss strengths in a flux shell per unit r (to be specified below). For any given physical quantity, the corresponding n^* is preserved under interchange motion in the absence of sources and sinks. For number density n, the corresponding n^* is the total number of ions in a flux tube, $Y \equiv NL^2$. The parameter L identifies the drift shell on which ions are drifting. For a dipole magnetic field, L is related to r by $L = r/\cos^2\theta$, where θ is the latitude. N is the total number of ions in the flux shell per unit L. For thermal energy density of an isotropic plasma, conservation of adiabatic invariants in a magnetic field implies that n^* is $NL^2TL^{8/3}$. The value of the diffusion coefficient, D, to be used in (1) is uncertain. It is usually assumed to be of the form $D_{LL} = K \cdot L^m$, where K and m are constants. We use $m = 3$

for the cold part of the torus ($L < 5.9$), and $m = 4$ for the warm part of the torus ($L > 5.9$). The way we have obtained the K-values of the cold and warm tori is described in the part of the model results. Table 1 summerizes the values of K and m. **Table 1.**

Local plasma source and loss terms are generally of the form $\alpha_{1,2} \cdot n_1 \cdot n_2$, where α is the reaction rate between species 1 and 2, and n_1 and n_2 are the number densities of each ion or neutral. These local rates must then be integrated over a flux tube to give $\mathcal{S}$ and $\mathcal{L}$ needed in (1). To perform this integration, one must know the distribution of a multi-species plasma along a field line.

If the temperature along a field line, $T_{\|}$ is constant, one may obtain an expression for the number density at a point s along the field line [*Bagenal and Sullivan*, 1981; *Mei et al.*, 1995]:

$$n_i(s) = n_{i,0} \cdot \exp\left[\left(1 - \frac{T_{\perp}}{T_{\|}}\right) \cdot \log\frac{B(s)}{B_0} + \frac{\frac{1}{2} m_i \Omega_J^2 \left(\rho^2(s) - \rho_0^2\right)}{T_{\|}} - \frac{Z_i q \left(\phi(s) - \phi_0\right)}{T_{\|}}\right] \tag{2}$$

Here $n_{i,0}$ is the equatorial density of species i, temperature is given in energy units, and q is the elementary charge. The first term, which is zero unless the plasma is anisotropic, is associated with the force generated by the magnetic mirror effect. The second term is the centrifugal force, where ρ is the distance from the spin axis, Ω_J is the rotation rate of Jupiter (taken to be that of the plasma), and m_i and n_i are the mass and number density of each ion species i. This force pushes the plasma outward along the field line and thus toward the equator. The third term is the force exerted by the ambipolar electric field set up by the interaction of plasma components of different mass and charge Z. This force causes heavy ions to be concentrated at the equator and lighter ions to have density maxima at higher latitudes. The ambipolar electric field is determined numerically by balancing the centrifugal and pressure gradient forces on the plasma. We neglect the contribution of Jupiter's gravity.

The source and loss terms in the diffusion equation (1) for the flux-tube-content of each of the plasma species are given by local source and loss terms integrated over the flux-tube-volume. The rate equation for the density of each ionic species n_j is written symbolically as

$$\mathcal{S} - \mathcal{L} = \int \left(\sum_{\alpha=i,e} \sum_{\beta=i,n} k_{\alpha\beta} n_\alpha n_\beta - \sum_{\substack{\alpha = i,e,n \\ j \neq i}} k_{\alpha j} n_\alpha n_j \right) d^3 r \ , \tag{3}$$

where the integration is over the flux tube. The double sum in the first term includes all mutual interactions of species α (denoting all ions and both thermal and suprathermal electrons) and species β (ions and neutrals) that produce species j with a rate coefficient $k_{\alpha\beta}$ (representing electron impact ionization and charge exchange). The second term accounts for chemical loss of species j. Table 2 lists the charge exchange reactions included in the model. Also included the reactions rates, k, at $L = 6$, based on theoretical calculations by *McGrath and Johnson* [1989]. At L-shells other than 6 they give the reactions rates according to the incident ion energy. **Table 2.**

The source and loss terms for the thermal energy content are similarly given as

$$\begin{aligned} \mathcal{S} - \mathcal{L} \ &= \ \int \left[\sum_{\alpha=i,e} \sum_{\beta=i} k_{\alpha\beta} n_\alpha n_\beta T_\beta - \sum_{\substack{\alpha = i,e,n \\ j \neq i}} k_{\alpha j} n_\alpha n_j T_j \right. \\ &\quad \left. + \sum_{\beta = pu\, ion} \nu^{\beta/j} n_\beta (T_\beta - T_j) - \nu^{j/e} n_j (T_j - T_e) \right] d^3 r \ . \end{aligned} \tag{4}$$

The first two terms represent energy reallocation because of a change of ion species. The third term corresponds to Coulomb energy transfer from pickup-ion species with $\nu^{\beta/j} = 1/\tau_{eq}^{\beta/j}$ given in appendix B. The fourth term corresponds to the loss of energy of species j to electrons via Coulomb energy transfer.

In the cold torus radial transport is slow and ion-electron recombination may affect the ionization distribution. In the hot torus the principal mechanism for recombination is dielectronic recombination, but radial transport is sufficiently fast to render all recombination processes negligible except for the case of S IV (see appendix A).

Johnson and Strobel [1982] demonstrated the importance of charge exchange reactions relative to other plasma processes, especially in the cold torus, where they found charge exchange processes to be the preferred mode for change of charge state of multiply charged ions, the dominant source of newly created ions and a major means of mass loss from the torus via the escape of fast neutrals. The temperature in the cold torus is very low because of the long residence times and the temperature dependence of the Coulumb collision rates. Rates of the charge exchange reactions included in the model are listed in appendix A.

For pickup ion species

$$\mathcal{S} - \mathcal{L} = \int \left[\sum_{\alpha=i,e} \sum_{\beta=n} k_{\alpha\beta} n_\alpha n_\beta T_\beta - \sum_{\substack{\alpha = i,e,n \\ j \neq i}} k_{\alpha j} n_\alpha n_j T_j \right. \\ \left. - \sum_{\beta=i,e} \nu^{j/\beta} n_j (T_j - T_\beta) - \nu^{j/e} n_j (T_j - T_e) \right] d^3 r \ . \quad (5)$$

The primary energy source for the system is $\beta = n =$ S or O. The temperature is given by the pickup energy of the ions created by initial ionization of a neutral with temperature given by

$$T_{pu} = \frac{1}{2} m_j V_{rel}^2 \ , \quad (6)$$

where

$$V_{rel} = \Omega_J r - \left(\frac{GM_J}{r} \right)^{1/2} \simeq 12.5L - 42/\sqrt{L} \ \ \mathrm{km\,s^{-1}} \quad (7)$$

represents the relative velocity of corotating plasma with respect to local Keplerian velocity. The newly created ions start life in a shell distribution which evolves via

Coulomb collisions to a Maxwellian characterized by a lower mean energy. The third term is the Coulomb energy transfer to thermal ion species and the fourth term corresponds to the loss of energy to electrons via Coulomb energy transfer.

The electron temperature is determined by balance between energy gain by Coulomb collisions with ions and energy loss by radiation:

$$\frac{\partial(n_e T_e)}{\partial t} = \sum_{\beta=i} \nu^{\beta/e} n_j (T_\beta - T_e) - \sum_{\beta=i,\lambda} \rho_{\beta,\lambda}\, n_e n_\beta \cdot \frac{hc}{\lambda} = 0\ . \tag{8}$$

The primary energy loss from the system is contained in the radiative cooling loss function corresponding to collisional excitation and radiative relaxation of the radiative rate coefficient ρ given in equation (10) below.

A substantial part of the pick-up energy is lost by radiative cooling which follows collisional excitation of the low-lying energy levels of the torus ions. The total collisional de-excitation rate per unit volume is given by *Osterbrock* [1989]

$$n_e n_2 q_{21} = n_e n_2 \left(\frac{2\pi}{T_e}\right)^{1/2} \frac{\hbar^2}{m_e^{3/2}} \frac{\Omega(1,2)}{\omega_2} \quad [\mathrm{cm}^{-3} \cdot \mathrm{sec}^{-1}]\ . \tag{9}$$

Here q_{21} is the collisional transition rate from level 2 to level 1 per particle in level 2 per colliding particle per unit volume per unit time, n_1 and n_2 are the ion concentration in the lower level and upper level, respectively, $\Omega(1,2)$ is the collision strength between levels 1 and 2, and ω_2 is the statistical weight of level 2.

The radiated power per unit volume is

$$n_e n_i \rho \cdot h\nu = n_e n_i \frac{8 \times 10^{-8}}{\sqrt{T_e}} \cdot \frac{\Omega \cdot h\nu}{\omega} e^{-h\nu/T}\ , \tag{10}$$

where both T_e and $h\nu$ are given in electron-volts, and ω is the degeneracy of the ground term. This equation defines ρ in equation (8).

The plasma species included in the model are thermal ions of S^+, S^{++}, S^{3+}, O^+, and O^{++}, thermal electrons, and pick-up of S^+, S^{++} and O^+. A small concentration of protons (their source is thought to be the Jovian ionosphere) is included. *Bagenal* [1994] set an upper limit on the proton density of $\sim 0.5\%$ in the cold torus, and *Tokar et al.* [1982] placed limits of 10-15% on the proton density in the warm torus. We adopt the values of *Bagenal* [1994] and do not include them in the list of the chemical interactions with the other species because their influence is small, so their presence does not significantly alter conclusions [*Barbosa*, 1994].

A small number density of hot electrons is included, as in the numerical model of *Barbosa* [1994] and the empirical model of *Bagenal* [1994]. Their density and temperature profiles were taken from the empirical model of *Bagenal* [1994].

Each ion and electron component requires an equation of the form 3 and 4. The resulting set of equations is closed by the condition of charge neutrality. The densities are then summed over latitude to find N, the number of ions in a magnetic flux shell per unit L.

The primary components of the neutral cloud are sulfur and oxygen atoms derived from the parent SO_2 molecule. The spatial distribution of neutral atoms is one of the basic model parameters. The radial structure of the neutral clouds was chosen to yield the proper distribution of plasma density. A cut along the equator through the neutral clouds gives density profiles as shown in figure 1. **Figure 1.**

For the reaction rates described in appendix A, the local rate of density change for atomic sulfur and oxygen at each L-value is given by:

$$\begin{aligned} -\frac{\partial n_{neutrals}}{\partial t} &= \left(I_S \cdot n_e + I_S^h \cdot n_{e,hot}\right) n_S + \left(I_O \cdot n_e + I_O^h \cdot n_{e,hot}\right) n_O \\ &\quad + \left[k_2 n_{S^{++}} + k_4 n_{S^{3+}} + (k_{10} + k_{11}) n_{O^{++}}\right] n_S \\ &\quad + \left(k_6 n_{O^{++}} + k_{12} n_{S^{++}} + k_{14} n_{S^{3+}}\right) n_O \qquad (11) \end{aligned}$$

In a similar way, the volume energy injection rate can be found from:

$$\begin{aligned} \frac{\partial (n_i \cdot T_i)}{\partial t} &= \left(I_S \cdot n_e + I_S^h \cdot n_{e,hot}\right) n_S \cdot T_{S^+_{pu}} \\ &\quad + \left(I_O \cdot n_e + I_O^h \cdot n_{e,hot}\right) n_O \cdot T_{O^+_{pu}} \\ &\quad + \left[k_2 n_{S^{++}} + k_4 n_{S^{3+}} + (k_{10} + k_{11}) n_{O^{++}}\right] n_S \cdot T_{S^+_{pu}} \\ &\quad + \left(k_6 n_{O^{++}} + k_{12} n_{S^{++}} + k_{14} n_{S^{3+}}\right) n_O \cdot T_{O^+_{pu}} \; . \qquad (12) \end{aligned}$$

Implementation

The model described here is based on the treatment given by *Richardson* [1992] for radial diffusion with integration of plasma along magnetic field lines

[*Bagenal and Sullivan*, 1981; *Richardson and Sittler, Jr.*, 1990] to provide a two dimensional model of plasma processes modified to calculate the ion and electron temperatures. The model's uniqueness lies in the use of the a distributed source of ions and energy, separation between thermal and pickup ions and the inclusion of most of the atomic processes known to occur in the torus.

The geometry of the inner Jovian magnetosphere is modeled by dividing the space around Jupiter into radial, R, and angular, θ, regimes. Grid points are located radially every 0.1 $\mathrm{R_J}$ in the range 5 to 10 $\mathrm{R_J}$, and the centrifugal latitude, θ, is incremented in steps of $\Delta\theta = 1°$ to a maximum latitude of 20°. The 10° tilt of the magnetic axis relative to the rotation axis is ignored, and an azimuthal symmetry with respect to these axes assumed. For any of the boxes defined by the grid points, rate processes of ionization, recombination, charge exchange, energy transfer and radiative loss are calculated. Since the assumption that the temperature remains constant along a field line is only valid for low latitudes, the model should not be relied on to provide densities above $\sim 20°$ latitude. Above $\sim 33°$ the field lines bend over (i.e., z decreases with θ). The volume of the flux tube decreases as $\cos^7\theta$ so that the high latitude plasma contributes proportionally less to the important integral quantities (e.g., NL^2 or average T_i, etc.).

Since the atomic reactions which are plasma sources and losses depend on the local number densities of the ions, electrons, and neutrals, whereas the rate of diffusion depends on the integrated quantity NL^2, a rigorous treatment of plasma transport must continuously shift between the use of number densities to calculate sources and losses and integrated quantities to calculate transport.

In the numerical code, the integrated quantities N_i are used to find the radial movement of plasma ($\partial Y/\partial t \propto \partial^2 Y/\partial L^2$). Then the number density of each plasma component is calculated as a function of latitude using (2), the source and loss of each plasma component are found at each latitude and the resulting number densities are summed to find N again for use in the diffusion equation. This is complicated by the fact that no equation directly relates the integrated quantity N

to the number density at any particular latitude. Thus an iterative scheme must be used to go from N to n; initial values of n_i are chosen, integrated over latitude to find the resulting N_i, compared with N_i obtained from the diffusion equation, the initial n_i values are adjusted, and this cycle is repeated until a consistent solution is reached. A schematic diagram showing the calculation scheme is shown in figure 2. **Figure 2.**

As boundary conditions for the diffusion equation, the electron densities are set fixed at $L = 5$ and $L = 10$. The density is integrated in latitude from the equator to 20°. The parallel temperature of the hot population is completely unknown. As in *Bagenal* [1994] we have taken a value of 5 for the anisotropy to be the standard.

Model results

Once the morphology (radial and vertical profiles) of the neutral cloud has been determined, a "calibration" of the model is needed; the constant K of the diffusion rate must be chosen. In order to obtain the value that will result in the best fit to the **flux-tube-content profile** of the empirical model of *Bagenal* [1994], both K and neutral cloud distribution are adjusted. Neutral cloud density was modeled so that $n_O/n_S \approx 3$ near Io's orbit, a sharp power low decrease (of the order of 6) outwards of Io's orbit (both radial and latitudinal), and a much sharper decrease inwards of Io's orbit. Then the value of K was varied with a fixed neutral cloud. Figure 3 show a comparison between the numerical model flux-tube-content profile obtained using the K-value given in table 1 and the empirical model profile. The model solution is in steady state and the sensitivity of this solution to variations in torus conditions is a subject of further work which is now on-going.

A weak point of the model can be inferred from the poor correspondence between the above profiles in the part of the cold torus. It is most reasonable that the cold torus needs to be treated with a model having much higher resolution (both radial and latitudinal). **Figure 3.**

The radial profile of the ion source rate, obtained by integrating equation

(11) over the flux tube is shown in figure 4 (solid line). The total ion source rate (the area under the line) is $\sim 3 \times 10^{28}$ ions/sec. This result is in good agreement with the hypothesis of the pickup energy as the main energy source for the torus; assuming the average pickup ion energy is $\sim$ 400 eV and the total torus emission is 2 TW, the ion source rate should be 3.125×10^{28} ions/sec. **Figure 4.**

The integral of equation (12) over the flux tube gives us the rate of energy input into the torus, which is also shown in figure 4 (dashed line). The available power of the torus (the area under the line) is $\sim 2 \times 10^{12}$ W. We conclude,therefore, that a neutral cloud of the form described in the previous chapter, results in an almost uniform energy source, spread at least to $10R_J$, and that the radiative efficiency of the torus is almost 90% (see next section).

The life-time of the neutral atoms against ionization and charge exchange can be found from the ratio of the neutral atoms flux-tube-content, $N_{neutral}$, to the neutral atoms flux-tube-content loss rate, $\partial N_{neutral}/\partial t$, multiplied by $(1+x)$, where x is the ratio of the charge exchange and electron impact ionization rates, i.e.:

$$\tau_{neutral} = \frac{N_{neutral}}{(1+x) \cdot \frac{\partial N_{neutral}}{\partial t}} .$$

The factor $(1+x)$ comes from the fact that about $x/(1+x)$ of the neutral atoms are lost via charge exchange with ions, a process which does not change the ion number density, and only $1/(1+x)$ of the neutral atoms are lost via electron impact ionization, a process which increases the ion number density. The low temperature in the cold torus results in a low loss rate of neutral atoms, and thus in a long life-time, of more than 10 hours. The neutral atom profile shown in figure 1 creates a life-time of $\sim$ 1 hour in the hot torus.

The ion transport rate (or, equivalently, ion residence time) has been inferred in several ways with apparently discrepant results. *Siscoe and Summers* [1981] estimated the diffusion rate, D_{LL}, in the torus as $D_{LL} \approx 1$ to 4×10^{-6} s^{-1}. *Smith and Strobel* [1985]] estimated the residence time, τ_D, as 5×10^6 seconds (or 60 days). Based on spectroscopic observations, *Shemansky* [1980] and *Moos et al.* [1985] deduced from the presence of highly ionized species a longer residence time

($\geq 9 \times 10^6$ seconds or 100 days).

For a quantitative estimate of the ion residence time in the warm torus, equation (1) yields [*Cheng*, 1986]

$$\frac{d}{dL}\left[\frac{D_{LL}}{L^2} \cdot \frac{d(NL^2)}{dL}\right] = -\frac{N}{\tau_D} \ . \tag{13}$$

This is now integrated from the maximum of NL^2 near $L_{in} = 5.8$ (where $d(NL^2)/dL = 0$) out to the torus outer boundary, L_{out}:

$$\frac{D_{LL}}{L^2} \cdot \left.\frac{d(NL^2)}{dL}\right|_{L_{out}} = -\frac{\int_{L_{in}}^{L_{out}} N\, dL}{\tau_D} \ . \tag{14}$$

The quantity τ_D was calculated for several values of L_{out} and is given in table 3. The values obtained here are in good agreement with previous estimates. It is also interesting to notice that the residence time in the range $7 \leq L \leq 8$ is only one third of the residence time in the range $5.8 \leq L \leq 7$. **Table 3.**

By running the code with a magnetosphere initially empty of ions until a steady state is reached, one can find the creation time of the torus to be $\sim 4 \times 10^7$ seconds (or 500 days).

Temperatures

After determination of the diffusion coefficient, only a few variables are left unconstrained. These are the neutral cloud distributions and the density and temperature of hot electrons.

Figure 5 shows the thermal electron temperature profile calculated from the model and compared with the measured one. The calculated electron temperature, which can be found by solving the radiative equilibrium equation lies below the measured temperature, especially at the location of the "ramp". This leads us to propose an external heat source that causes the observed increase in T_e. **Figure 5.**

Computed temperatures for all thermal species are shown in figure 6. The calculated average ion temperature (of both thermal and suprathermal species) matches the *in situ* measusred temperature very well. Figure 7 shows temperature profiles of pickup species compared with the energies of locally picked up O^+ and S^+ ions. The calculated temperatures are of course lower than the pickup energies because part of the energy has been transferred to the thermal ions and electrons. **Figure 6.**

Figure 7.

The temperature profiles lead us to ask why all the thermal ions do not share the same temperature, and what rule determines the deviation of the pickup ions from the pickup energy.

We assume the pickup ions move through a uniform background of thermal ions and electrons. The rate at which a pickup ion transfers part of its energy (via Coulomb collisions with the ambient plasma) is determined by τ_{eq} (equation B2). Because $\tau_{eq}^{\alpha/\beta} \propto 1/Z_\beta^2$,

$$\tau_{eq}^{\alpha/S_{pu}^{++}} = \frac{\tau_{eq}^{\alpha/S_{pu}^{+}}}{4} ,$$

i.e., S_{pu}^{++} transfer energy at a much higher rate, and thus pickup S^{++} deviate from the corotation energy much more than do the pickup S^+ ions.

The energy balance of each thermal ion is determined (mainly) by its ability to absorb energy from the pickup ions (source). A comparison of thermal equilibration times shows that $\tau_{eq}^{pickup\ ion/thermal\ ion} \propto 1/(Z_{thermal}^2 \cdot n_{thermal}^2)$, thus, $\tau_{eq}^{pickup\,/O^{++}} \approx 20 \cdot \tau_{eq}^{pickup\,/O^{+}}$. Therefore, thermal ions with high charge state and/or low abundance (such as O^{++}, S^+, and S^{3+}) will be colder than the much more abundant species (O^+, and S^{++}). Outside of the warm torus, ion number densities are low enough so that Coulomb thermalization becomes negligible.

Ion partitioning

Figure 8 shows radial profiles of electron and ion density at the centrifugal equator obtained from the model and compared with those given by the empirical model of *Bagenal* [1994]. Figure 8 also shows the same profiles assuming the electron temperature is the *in situ* one (i.e., not modified by the model). The increase in T_e at the location of the "ramp" changes the ion partitioning significantly; the abundance of S_{pu}^+, O_{pu}^+, S^{3+} and O^{2+} increases at the expense of other ionization states. **Figure 8.**

The calculated radial profile of the $[S^+]/[S^{++}]$ ratio is given in figure 9a. In part (b) of the figure, the ratio $[O^{++}]/n_e$ is shown. The ratio of ion density to electron density as a function of radial distance is shown in part (c). **Figure 9.**

Figure 9a shows clearly that the model can account for the observed requirement that [S II]/[S III] <1 in the warm torus. *Pilcher and Morgan* [1985] have observed high-density plasma (at some occasions $n_e \approx 10^4$ cm^{-3}) with an estimated [S II]/[S III] ≈ 0.6. The Neutral Cloud Theory of *Barbosa et al.* [1983] predicts a high ratio of [S II]/[S III] together with low T_e (~ 3 eV). We conclude that Neutral Cloud Theory can account for a torus with ionization states higher than 1, using electron temperature as low as ~ 3.6 eV.

The calculated mixing ratio of O^{++} (figure 9b) is not as high as reported by *Bagenal et al.* [1992] (~ 0.2 at L=10). *Bagenal* [1989] and *Bagenal et al.* [1992] argue that the Voyager observations of higher plasma temperatures and enhanced oxygen composition support a Europa source. *Schreier et al.* [1993] present a theoretical model suggesting that the Europa source is probably less than the Io source by a factor of 10, but could produce significant changes in composition and temperature, that might explain the high mixing ratio of O^{++}.

The average ion charge (figure 9c) increases with increasing L out to $L \sim 8$, and then remains at a constant value of $\sim 3/2$. This is of course related to the increase in the electron temperature; beyond $8R_J$, chemical processes are dominated by diffusion, and thus no changes occur in the ionization states.

Emission

Figure 10 is a profile of the radiated power. The solid line indicates the radiated power using the empirical model ion and electron densities and temperatures. The dash-dotted line indicates radiated power obtained by using the numerical model ion and electron densities, but with electron temperatures left unchanged. The dashed line indicates the radiated powerobtained from the numerical model ion and electron densities and temperatures. The numbers in parenthesis are the total torus emitted power in TW. It is seen that if the electron temperature is decreased from $\sim$ 5eV (observed) to $\sim$ 3.6eV, (predicted by numerical calculations), the total observed UV emission ($\sim$ 2 TW) observed by the Voyager spacecraft cannot be accounted for. This model, based on Neutral Cloud Theory, fails (as do many previous models) to explain one of the most important features of the torus - its high radiated power. **Figure 10.**

Summary and conclusions

In the model presented here, we have calculated plasma properties in the Io torus by including radial diffusion, chemical and radiation processes, and a distributed source. The number of free parameters in the model is quite small; the neutral cloud profile, the diffusion coefficient and the number density of the hot electrons. Other properties such as the density and temperature of the hot electrons and the thermal protons were adopted from the empirical model of *Bagenal* [1994].

To the extent that the radial diffusion coefficient, D_{LL}, scales with L according to a power law: $D_{LL} = K \cdot L^m$, where $m \approx 4$ [*Siscoe et al.*, 1981] the D_{LL} values given by the model ($K = 3.6 \times 10^{-10}$), are 4.7×10^{-7}, 8.6×10^{-7}, 1.5×10^{-6} and 2.4×10^{-6}, at $L = 6$, 7, 8 and 9, respectively. *Cheng* [1986] has estimated D_{LL} to be about 1 to 4×10^{-6} sec^{-1} in the regions around $L = 7$ to 8. An upper limit for D_{LL}, 10^{-5} sec^{-1}, was obtained by *Gehrels and Stone* [1983] for the 8 to $9R_J$ region and an expected value was about 4×10^{-6} sec^{-1}. Phase space density analyses for electrons in the 6 to $10R_J$ regions performed by *Ye and Armstrong* [1993] imply a diffusion coefficient that is substantially below 10^{-6} sec^{-1}.

The general increase with increasing L in temperature of both ions and electrons is contrary to what is expected from adiabatic expansion, which should cool the plasma as it expands on diffusing outwards, away from the source near Io. It has recently been suggested [*Thomas and Lichtenberg*, 1997] that this increase may be wholly or in part a result of latitudinal selection effects in the empirical model; it this possibility is disregarded, however, one must conclude that there is a continuous process of mass and energy loading. In the calculated model, the distributed nature of the neutral clouds is responsible for the increase. On the assumption that all thermal ions have the same temperature (i.e. $T_{S^+} = T_{S^{++}} = ... = T_{O^{++}} \equiv T_i$), the energy source is given by:

$$\frac{\partial}{\partial t}\left(\sum_{i=thermal}(n_i T_i) + \sum_{j=pu}(n_j T_j) + n_e T_e\right) = \tag{15}$$

$$\left(I_S \cdot n_e + I_S^h \cdot n_{e,hot} + k_2 n_{S^{++}} + k_4 n_{S^{3+}} + k_{10} n_{O^{++}}\right) n_S \cdot T_{S^+,pu}$$
$$+ \left(I_O \cdot n_e + I_O^h \cdot n_{e,hot} + k_6 n_{O^{++}} + k_{12} n_{S^{++}} + k_{14} n_{S^{3+}}\right) n_O \cdot T_{O^+,pu}$$
$$+ k_{11} n_{O^{++}} n_S \cdot T_{S^{++},pu} + (k_1 n_S n_{S^+} + k_9 n_O n_{O^+}) \cdot (T_{S^+,pu} - T_i)$$
$$+ k_3 n_S n_{S^{++}} \cdot (T_{S^{++},pu} - T_i) + n_O \cdot (k_5 n_{O^+} + k_8 n_{S^+}) \cdot (T_{O^+,pu} - T_i)$$
$$+ k_7 n_{O^{++}} \cdot (T_{O^{++},pu} - T_i) - \sum_i \rho_i n_e n_i \tag{16}$$

Equating the neutral densities to zero will lead to a negative energy injection rate, as expected in the diffusion-dominated case.

The shape of the neutral cloud, though it is for the most part confined to Io's orbit, suggests an almost uniform energy source. From a total available power of $\sim 2 \times 10^{12}$ W, the model torus was found to emit 85% via radiation, under the assumption that the measured electron temperature is the one that exists *in situ*. The calculated electron temperature cannot account for the 2-3 TW radiation found by the UVS instrument on board the two Voyager spacecraft. The model emission profile does not show confinement of the emission to the narrow band in the hot torus between 5.6 and $6.0 R_J$ called the "ribbon" region [*Trauger*, 1984] but rather predicts that the emission will spread outward to $7.0 R_J$. *Taylor et al.* [1995] have developed a sophisticated code (named CITEP) to simulate emissions from the Io plasma torus, and have used it to examine the consistency of Voyager PLS and UVS observations. Using torus plasma parameters derived by *Bagenal* [1994] the program predicts the brightness and morphology of torus EUV emissions. *Taylor et al.* [1995] find that the measured brightness is approximately twice as large as the CITEP code predicts. Their radial emission profile is less sharply peaked at the "ribbon" location than the observed profile.. Table 4 lists electron collision strengths of several prominent emission lines used to compute the radiative loss function, using equation (10). The collision strengths listed in this table will certainly be subject to revision in the future. **Table 4.**

The resulting 2-D profiles of densities and temperatures resemble those presented by the empirical model of *Bagenal* [1994] except for that of the electron temperature. The description of plasma properties in the cold part of the torus should be taken only qualitatively, because higher resolution is needed to account for features such as the "ribbon".

The inability of our present model to account for the measured torus radiation indicates that an external heat source that will raise the electron temperature from 3.6 to 5 eV should be invoked. Three different mechanisms can be suggested:

- an increase in the temperature or the density of the thermal ions that will result in electron heating via Coulomb collisions,
- hot ions (with energies $\geq$ keV), presumably of ring current origin, diffusing inwards and heating the thermal electrons
- a flux of suprathermal electrons.

In order to model these possibilities, we used plasma parameters at a single location ($L = 6$), and changed (or added) various features in the radiative equilibrium equation.

The first test was to find the temperature of thermal ions required to account for the observed T_e. Figure 11 shows that T_e changes slowly from 3.6 to 5 eV, as the thermal ion temperature increases from $\sim$ 60 eV to the unreasonable value of $\sim$ 230 eV, . This high value of $T_{i,thermal} > 200$ eV is needed because the energy transfer rate is small. **Figure 11.**

Smith et al. [1988] have suggested that the required external energy input is carried into the torus by inward radial diffusion of low-density hot ions. We have added an external O^+ component with energy varying from 1 to 10 keV to the radiative equilibrium equation. Figure 12 shows the number density of energetic O^+ particles required to account for the increase of the thermal electron temperature from 3.6 to 5 eV; at energies ≥ 6 keV, the charge fraction of the energetic particles is < 0.025. **Figure 12.**

The plasma torus is known to contain a non-Maxwellian electron distribution [*Scudder et al.*, 1981; *Sittler Jr and Strobel*, 1987]. *McNutt Jr. et al.* [1990] attributed them to secondary (backscattered) electron production by intense Jovian auroral energetic particle precipitation, and *Barbosa* [1994] suggests that they are a consequence of wave-particle interactions between the thermal and the extremely nonthermal parts of the plasma distribution.In his model he included a small population ($\sim 0.2\%$) of suprathermal electrons with $\sim$ keV energies, and found they have a substantial influence on the ionization balance of the torus plasma. Barbosa does not show model results of a torus in which suprathermal electrons are absent, and we did not succeeded in reconstructing the 'pronounced effect' these electrons have on the ionization state. Rather, we saw that charge exchange and ionization by thermal electrons are the main mechanisms for enhancing the plasma charge state.

Investigating the role of suprathermal electrons on the torus radiation we have added a hot component to the radiative equilibrium equation. We have varied their number density in order to find the critical abundance of hot electrons required to cause the temperature increase of the thermal electrons. Intuitively, one would expect that as the temperature of the suprathermal electrons increases, fewer suprathermal electrons are needed. The relaxation rate of the suprathermal electrons varies with their energy, $T_{e,hot}$, as $\nu^{e,hot/e,thermal} \propto (T_{e,hot} + T_{e,thermal})^{-3/2}$; the energy transfer rate varies with $T_{e,hot}$ as

$$\nu^{e,hot/e,thermal} \cdot (T_{e,hot} - T_{e,thermal}) \propto \frac{T_{e,hot} - T_{e,thermal}}{(T_{e,hot} + T_{e,thermal})^{3/2}} .$$

This energy transfer rate has a maximum value at $T_{e,hot} \approx 5\, T_{e,thermal}$, and falls off as $T_{e,hot}$ is increased. Figure 13a shows the number density of the suprathermal electrons required to account for the temperature increase in the thermal electrons as a function of $T_{e,hot}$. It is seen that the use of high-energy electrons will result in a great abundance of these electrons due to a low relaxation rate, while an anomalous energy transfer rate occur at energies of $T_{e,hot} \approx 25$ eV. *Thorne* [1981] predicts that heavy ion precipitation into the Jovian upper atmosphere will result in the production of secondary electrons with a mean energy in the range 20-40 eV. **Figure 13.**

Because the relaxation times between hot and thermal electrons are short ($\sim$ 20 hr.) compared with relaxation times between pickup ions and thermal electrons ($\sim$ 10 days), a continuous supply of hot electrons is required for a continuous torus emission of $\sim$ 2 TW. Figure 13b shows that a minimum electron flux of $10^9 \mathrm{cm}^{-2}\,\mathrm{s}^{-1}$ or a number density of $\approx 8 \mathrm{cm}^{-3}$ is needed to maintain the strong torus emission. This number density which is about 0.5% of the thermal electron density is not unreasonable in itself. On the other hand, their fluxes are highly variable and the time variability of the torus emission predicted in this scenario is high. In the low-density hot O^+ component scenario, the torus emission variability is low, since these ions have to travel from Io's torus to the outer Jovian magnetosphere, and be accelerated there before diffusing inward back to the torus. We would expect, therefore,d that the hot electron mechanism would be less probable than the hot ion process.

In summary, of the three proposed heat input mechanisms, only the addition of hot plasma appears to be plausible. The other two mechanisms require excessive enhancements of either thermal ion temperature or suprathermal electron flux.

As T_e increases, the abundance of S^+_{pu}, O^+_{pu}, S^{3+} and O^{2+} increases at the expense of other ionization states. *Hord et al.* [1995] reported first results from the Extreme Ultraviolet (EUV) Spectrometer on board the Galileo spacecraft, obtained during the approach to Jupiter, for a total of 35 days between 10 October and 27 November 1995. They found $T_e \sim 6$ eV, torus luminosity of ≈ 2 TW, high mixing ratio of S^{2+} and S^{3+}, but no evidence for O^{2+}.

Our model does not reproduce the drop in the flux tube content in regions outside 5.7$\mathrm{R_J}$ found in the empirical model and attributed to the impoundment of the torus by ring current particles; the "ramp" is blurred out by rapid diffusion. The reality of the "ramp" in the empirical model itself, however, has been questioned on several different different grounds*Herbert and Sandel* [1995]; *Mauk et al.* [1996]; *Matheson and Shemansky* [1994].

Appendix A: Appendix A: Reactions included in the model calculations

Rate coefficients for electron impact ionization [$I_j(T_e)$ in cm^3 s^{-1}] are taken from *Brown et al.* [1983] with the exception of S I which has been revised using laboratory measurements [*Ziegler et al.*, 1982]. The best analytical representation of these data is given as follows:

$$I_S = 7.4 \times 10^{-8} \cdot \sqrt{T_e} \cdot \exp\left(-\frac{36}{T_e}\right) , \tag{A1}$$

$$I_S^h = 1.464 \times 10^{-6} \cdot \frac{\ln\left(T_{e,hot}/27.37\right)}{\sqrt{T_{e,hot}}} , \tag{A2}$$

$$I_{S+} = 1.274 \times 10^{-8} \cdot \sqrt{T_e} \cdot \exp\left(-\frac{23.1}{T_e}\right) , \tag{A3}$$

$$I_{S+}^h = 4.44 \times 10^{-7} \cdot \frac{\ln\left(T_{e,hot}/27.07\right)}{\sqrt{T_{e,hot}}} , \tag{A4}$$

$$I_{S++} = 5.8 \times 10^{-9} \cdot \sqrt{T_e} \cdot \exp\left(-\frac{34.88}{T_e}\right) , \tag{A5}$$

$$I_{S++}^h = 1.76 \times 10^{-7} \cdot \frac{\ln\left(T_{e,hot}/27.07\right)}{\sqrt{T_{e,hot}}} , \tag{A6}$$

$$I_O = 1.015 \times 10^{-8} \cdot \sqrt{T_e} \cdot \exp\left(-\frac{14.54}{T_e}\right) , \tag{A7}$$

$$I_O^h = 5.74 \times 10^{-7} \cdot \frac{\ln\left(T_{e,hot}/27.07\right)}{\sqrt{T_{e,hot}}} , \tag{A8}$$

$$I_{O+} = 3.78 \times 10^{-9} \cdot \sqrt{T_e} \cdot \exp\left(-\frac{33.42}{T_e}\right) , \tag{A9}$$

and

$$I_{O+}^h = 1.76 \times 10^{-7} \cdot \frac{\ln\left(T_{e,hot}/27.07\right)}{\sqrt{T_{e,hot}}} . \tag{A10}$$

Here I_j^h denotes the ionization rate of species j by suprathermal electrons.

The atomic data for radiative and dielectronic recombination given by *Brown et al.* [1983] indicate that recombination processes are slow compared with the diffusion transport time and may be neglected, with the exception of S IV. A recombination coefficient of the form

$$R_{S^{3+}} = 5.4 \times 10^{-11} \cdot T_e^{0.53} \tag{A11}$$

is employed for this ion.

Appendix B: Appendix B: Relaxation rates of thermal equilibration

The rate of change of temperature of species β in the presence of species α is described by *Spitzer* [1962]

$$\frac{dT_\beta}{dt} = \sum_\alpha \frac{(T_\alpha - T_\beta)}{\tau_{eq}^{\alpha/\beta}} \tag{B1}$$

where the equipartition time is:

$$\begin{aligned} \tau_{eq}^{\alpha/\beta} &= \frac{3 m_\alpha m_\beta}{8\sqrt{2\pi} n_\beta Z_\alpha^2 Z_\beta^2 e^4 \lambda_{\alpha/\beta}} \left(\frac{T_\alpha}{m_\alpha} + \frac{T_\beta}{m_\beta} \right)^{3/2} \\ &= 7.37 \times 10^6 \frac{(\mu_\alpha T_\beta + \mu_\beta T_\alpha)^{3/2}}{(\mu_\alpha \mu_\beta)^{1/2} Z_\alpha^2 Z_\beta^2 n_\beta \lambda_{\alpha/\beta}} \text{ sec.} \end{aligned} \tag{B2}$$

Here μ is the mass in units of the proton mass m_p, Z is the ion or electron charge state, $\lambda_{\alpha/\beta}$ is the Coulomb logarithm, T is given in electron-volts, and all units are cgs. If thermal ions have the same temperature, T_i, equation (B1) becomes

$$\frac{dT_\beta}{dt} = -\sum_i \frac{(T_\beta - T_i)}{\tau_{eq}^{\beta/i}} - \frac{(T_\beta - T_e)}{\tau_{eq}^{\beta/e}} ,$$

where

$$\sum_i \frac{1}{\tau_{eq}^{\beta/i}} = \frac{1}{\tau_{eq}^{\beta/S^+}} + \frac{1}{\tau_{eq}^{\beta/S^{++}}} + \ \ldots \equiv \frac{1}{\tau_{eq}^{\beta/i}}$$

Book [1977] gives convenient expressions for $\lambda_{\alpha/\beta}$ for mixed ion-ion collisions

$$\lambda_{\alpha/\beta} = 23 - \ln \left[\frac{Z_\alpha Z_\beta (\mu_\alpha + \mu_\beta)}{\mu_\alpha T_\beta + \mu_\beta T_\alpha} \left(\frac{n_\alpha Z_\alpha^2}{T_\alpha} + \frac{n_\beta Z_\beta^2}{T_\beta} \right)^{1/2} \right] , \tag{B3}$$

and for electron-ion collisions, where $\mu_e \to 0$ and $T_i m_e/m_i < T_e < 10 Z_i^2$ eV,

$$\lambda_{e/i} = \lambda_{i/e} = 23 - \ln \left(n_e^{1/2} Z_i T_e^{-3/2} \right) . \tag{B4}$$

Rate coefficients for the principal reactions in the torus are given in appendix A and in Table 2.

Acknowledgments. The work at Tel Aviv University and at the Max-Planck-Institut für Aeronomie was supported in part by the German-Israeli Foundation for Scientific Research and Development under grant I-0199-163.07/91. At the Johns Hopkins University Applied Physics Laboratory this research was supported by the NASA Galileo Program by means of contract N00039-95-0002 between the United States Department of the Navy and Johns Hopkins University. A. Eviatar gratefully acknowledges the hospitality of the Johns Hopkins University Applied Physics Laboratory.

References

Bagenal, F., Torus-magnetosphere coupling, in *Time-Variable phenomena in the Jovian System*, edited by M. J. S. Belton, R. A. West, and J. Robe, vol. SP-494, pp. 196–210. NASA, Washington DC, 1989.

Bagenal, F., Empirical model of the Io plasma torus: Voyager measurements, *J. Geophys. Res.*, *99*, 11,043–11,062, 1994.

Bagenal, F., and J. Sullivan, Direct plasma measurements in the Io torus and inner magnetosphere of Jupiter, *J. Geophys. Res.*, *86*, 8447–8466, 1981.

Bagenal, F., D. E. Shemansky, R. L. McNutt Jr., R. Schreier, and A. Eviatar, The abundance of O^{++} in the Jovian magnetosphere, *Geophys. Res. Lett.*, *19*, 79–82, 1992.

Barbosa, D. D., Neutral cloud theory of the Jovian nebula: Anomalous ionization effect of superthermal electrons, *Astrophys. J.*, *430*, 376–386, 1994.

Barbosa, D. D., F. V. Coroniti, and A. Eviatar, Coulomb thermal properties and stability of the Io plasma torus, *Astrophys. J.*, *274*, 429–442, 1983.

Book, D. L., *Revised and Enlarged Collection of Plasma Physics Formulas and Data*, Memo. Rep. 3322. Naval Res. Lab., Washington, D. C., 1977.

Brown, R. A., C. B. Pilcher, and D. Strobel, Spectrophotometric studies of the Io torus, in *Physics of the Jovian Magnetosphere*, edited by A. J. Dessler, Cambridge Planetary Science, pp. 197–225. Cambridge University Press, 1983.

Cheng, A. F., Radial diffusion and ion partitioning in the Io torus, *Geophys. Res. Lett.*, *13*, 517–520, 1986.

Dungey, J. W., Effects of the electromagnetic perturbations on particles trapped in the radiation belts, *Space Sci. Rev.*, *4*, 199–222, 1965.

Gehrels, N., and E. C. Stone, Energetic oxygen and sulphur ions in the Jovian magnetosphere and their contributions to the auroral excitation, *J. Geophys. Res.*, *88*, 5537–5537, 1983.

Herbert, F., and B. R. Sandel, Radial profiles of ion density and parallel temperature in the Io plasma torus during the voyager 1 encounter, *J. Geophys. Res.*, *100*, 19,513–19,529, 1995.

Hord, C. W., A. I. Stewart, C. A. Barth, W. E. McClintock, W. R. Pryor, K. E. Simmons, M. H. Taylor, J. M. Ajello, R. A. West, W. K. Tobiska, K. L. Naviaux, S. J. Edberg, B. R. Sandel, A. L. Broadfoot, D. M. Hunten, and D. E. Shemansky, The Galileo extreme ultraviolet spectrometer: First observations of Jupiter and the Io torus, *EOS*, *76*, 346, 1995.

Johnson, R. E., and D. F. Strobel, Charge exchange in the Io torus and exosphere, *J. Geophys. Res.*, *87*, 10385–10393, 1982.

Matheson, P. L., and D. E. Shemansky, Chemistry and transport in the Io torus ramp, *Icarus*, *unpublished*, 1994.

Mauk, B. H., S. A. Gary, M. Kane, E. P. Keath, S. M. Krimigis, and T. P. Armstrong, Hot plasma parameters of Jupiter's inner magnetosphere, *J. Geophys. Res.*, *101*, 7,685–7,695, 1996.

McGrath, M. A., and R. E. Johnson, Charge exchange cross sections for the Io plasma torus,, *J. Geophys. Res.*, *94*, 2677–2683, 1989.

McNutt Jr., R. L., F. Bagenal, and R. M. Thorne, Observations of auroral secondary electrons in the Jovian magnetosphere, *Geophys. Res. Lett.*, *17*, 291–294, 1990.

Mei, Y., R. M. Thorne, and F. Bagenal, Analytical model for the density distribution in the Io plasma torus, *J. Geophys. Res.*, *100*, 1823–1828, 1995.

Moos, H. W., T. E. Skinner, S. T. Durrance, and P. D. Feldman, Long term stability of the Io high temperature plasma torus, *Astrophys. J.*, *294*, 369–382, 1985.

Osterbrock, D. E., *Astrophysics of Gaseous Nebulae and Active Galactic Nuclei.* University Science Books, Mill Valley, CA, 1989.

Pilcher, C. B., and J. S. Morgan, Magnetic longitude variations in the Io torus, *Adv. Space Res.*, *5*, 337–, 1985.

Richardson, J., and E. Sittler, Jr., A plasma density model for saturn based on voyager observations, *9J. Geophys. Res.*, *95*, 12,019–12,031, 1990.

Richardson, J. D., A new model for plasma transport and chemistry at saturn, *J. Geophys. Res.*, *97*, 13,705–13,713, 1992.

Schreier, R., A. Eviatar, V. M. Vasyliunas, and J. D. Richardson, Modeling the Europa plasma torus, *J. Geophys. Res.*, *98*, 21,231–21,243, 1993.

Scudder, J. D., E. C. Sittler Jr., and H. S. Bridge, A survey of the plasma electron environment of Jupiter: A view from Voyager, *J. Geophys. Res.*, *86*, 8157–8179, 1981.

Shemansky, D. E., Mass-loading and diffusion-loss rates of the Io plasma torus, *Astrophys. J.*, *242*, 1266–1277, 1980.

Shemansky, D. E., Energy branching in the Io plasma torus: The failure of neutral cloud theory, *J. Geophys. Res.*, *93*, 1773–1784, 1988.

Siscoe, G. L., and D. Summers, Centrifugally driven diffusion of Iogenic plasma, *J. Geophys. Res.*, *86*, 8471–8479, 1981.

Siscoe, G. L., A. Eviatar, R. M. Thorne, and J. D. Richardson, Ring current impoundment of the Io plasma torus, *J. Geophys. Res.*, *86*, 8480–8484, 1981.

Sittler Jr, E. C., ., and D. F. Strobel, Io plasma torus electrons, *J. Geophys. Res.*, *92*, 5741–5762, 1987.

Smith, R. A., and D. F. Strobel, Energy partitioning in the Io plasma torus, *J. Geophys. Res.*, *90*, 9469–9493, 1985.

Smith, R. A., F. Bagenal, A. F. Cheng, and D. F. Strobel, On the energy crisis in the Io plasma torus, *Geophys. Res. Lett.*, *15*, 545–548, 1988.

Spitzer, L., *Physics of fully ionized gases.* Interscience, New York, 1962.

Taylor, M. H., N. M. Schneider, F. Bagenal, B. R. Sandel, D. E. Shemansky, P. L. Matheson, and D. T. Hall, A comparison of the voyager 1 ultraviolet spectrometer and plasma science measurements of the Io plasma torus, *J. Geophys. Res.*, *100*, 19541–19550, 1995.

Thomas, N., and G. Lichtenberg, The latitudinal dependence of ion temperature in the Io plasma torus, *Geophys. Res. Lett.*, *24*, 1175–1178, 1997.

Thorne, R. M., Jovian auroral secondary electrons and their influence on the Io plasma torus., *Geophys. Res. Lett.*, *8*, 509–512, 1981.

Tokar, R., D. A. Gurnett, and F. Bagenal, The proton concentration in the vicinity of the Io plasma torus, *J. Geophys. Res.*, *87*, 10,395–10,400, 1982.

Trauger, J. T., The Jovian nebula: A post-voyager perspective, *Science*, *226*, 337–341, 1984.

Ye, G., and T. P. Armstrong, Electron distributions in the inner Jovian magnetosphere: Voyager 1 observations,, *J. Geophys. Res.*, *98*, 21253–21253, 1993.

Ziegler, D. L., J. H. Newman, L. N. Goeller, K. A. Smith, and R. F. Stebbings, Single and multiple ionization of sulfur atoms by electron impact, *Planet. Space. Sci.*, *30*, 1269–1274, 1982.

This manuscript was prepared with the AGU LaTeX macros v3.1.

With the extension package 'AGU^{++}', version 1.2 from 1995/01/12

Figure Captions

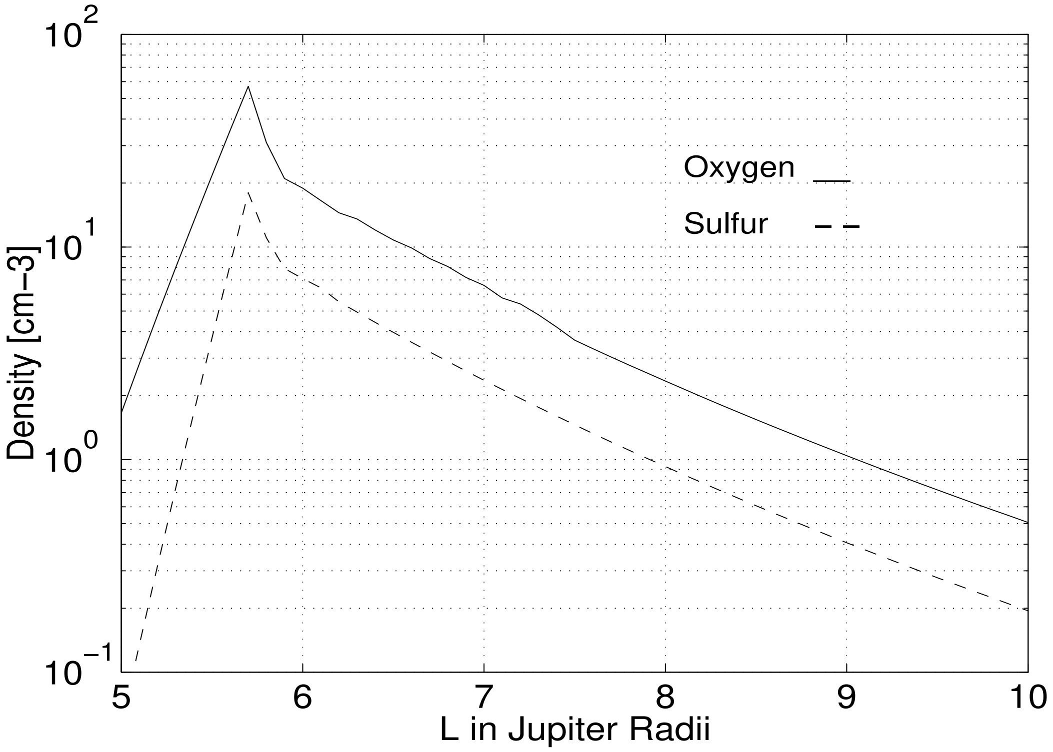

Figure 1. Density profile of neutral oxygen and sulfur along the equator.

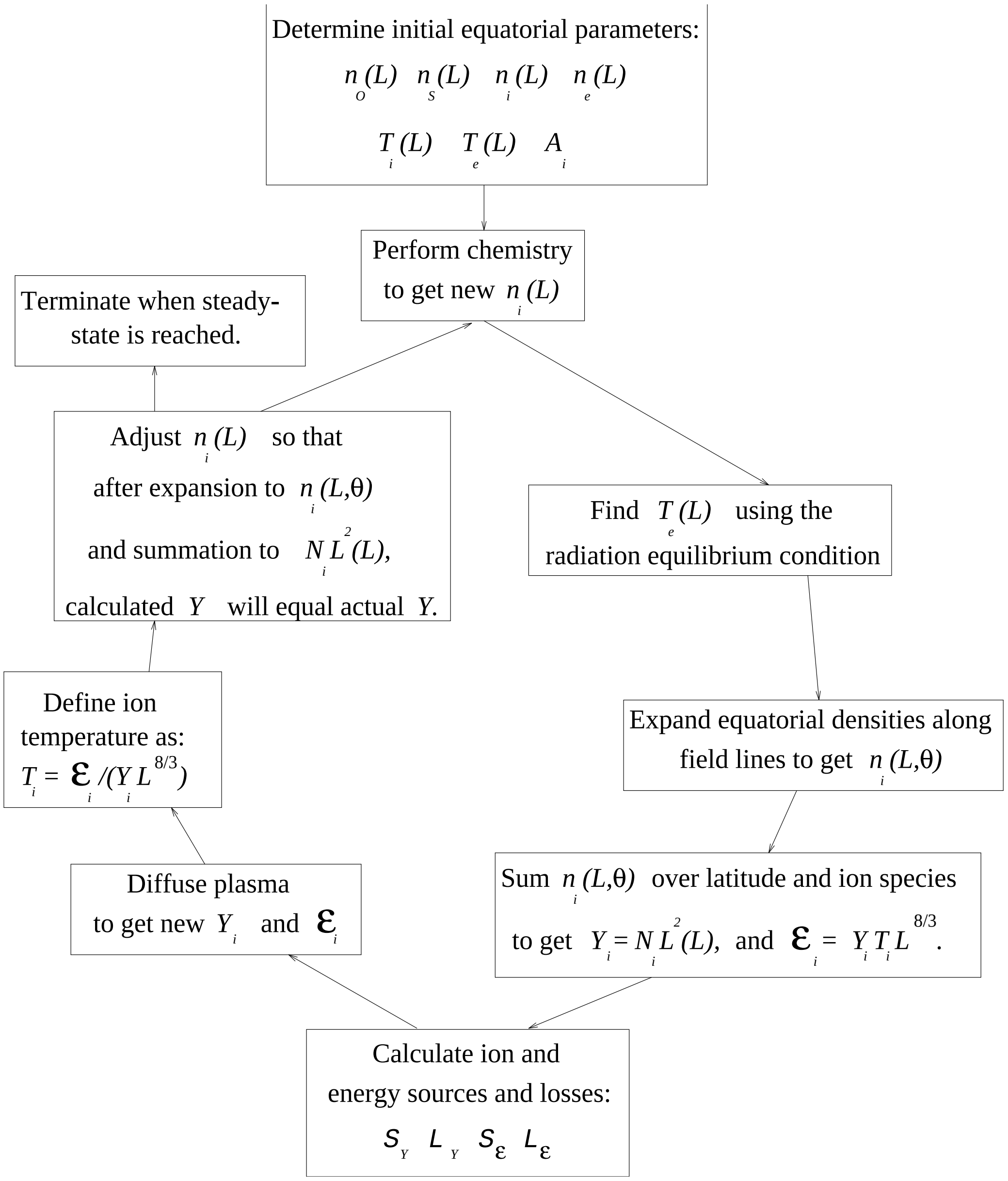

Figure 2. Schematic diagram showing a flow chart of the model calculations used.

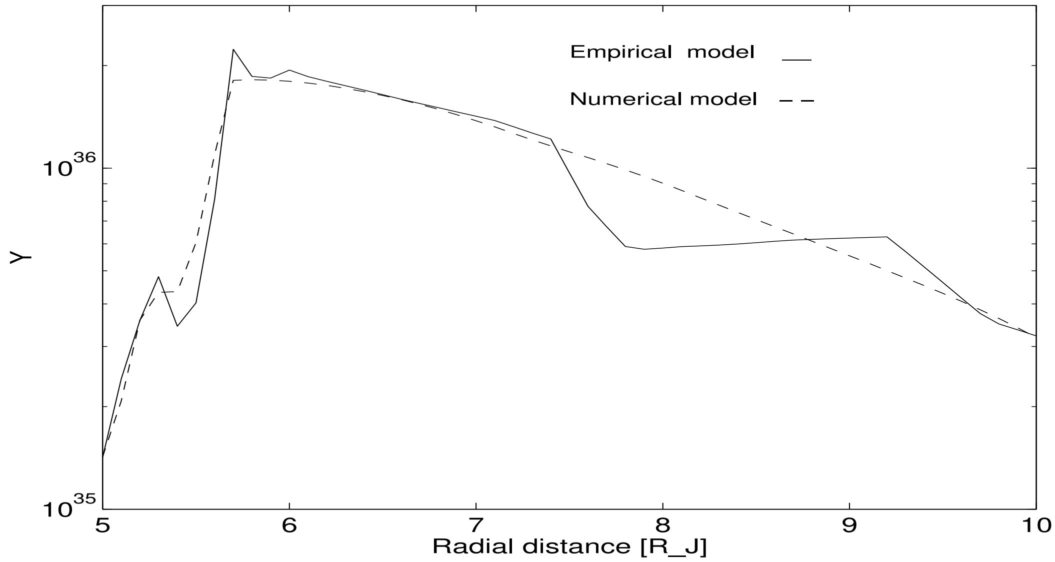

Figure 3. A comparison between the flux tube content profile as given by the empirical model of *Bagenal* [1994] (solid line), and the numerical model (dashed line).

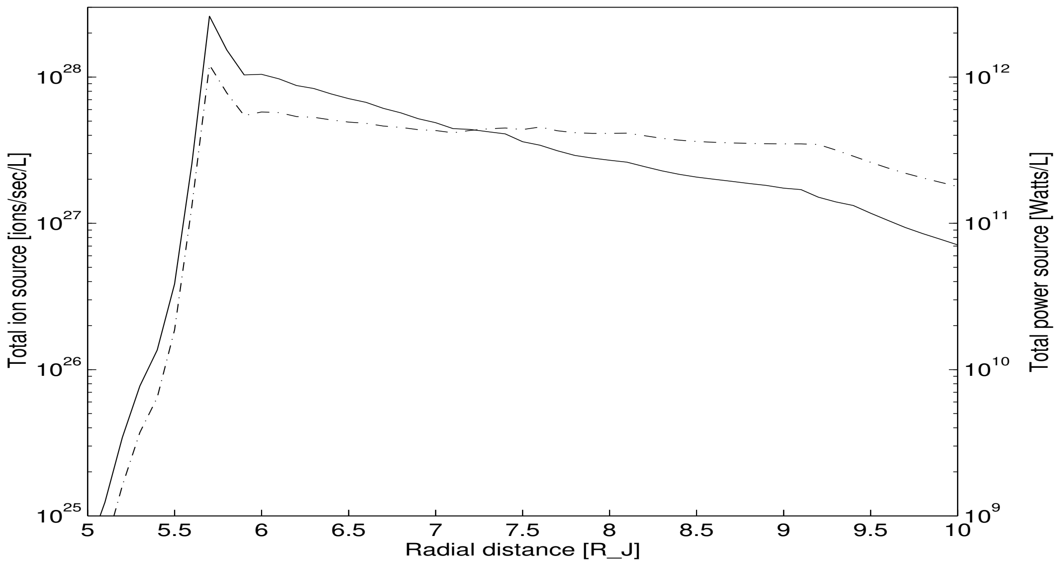

Figure 4. Total ion source rate in ions per sec per unit L (solid line), and total power source in W per unit L (dashed line).

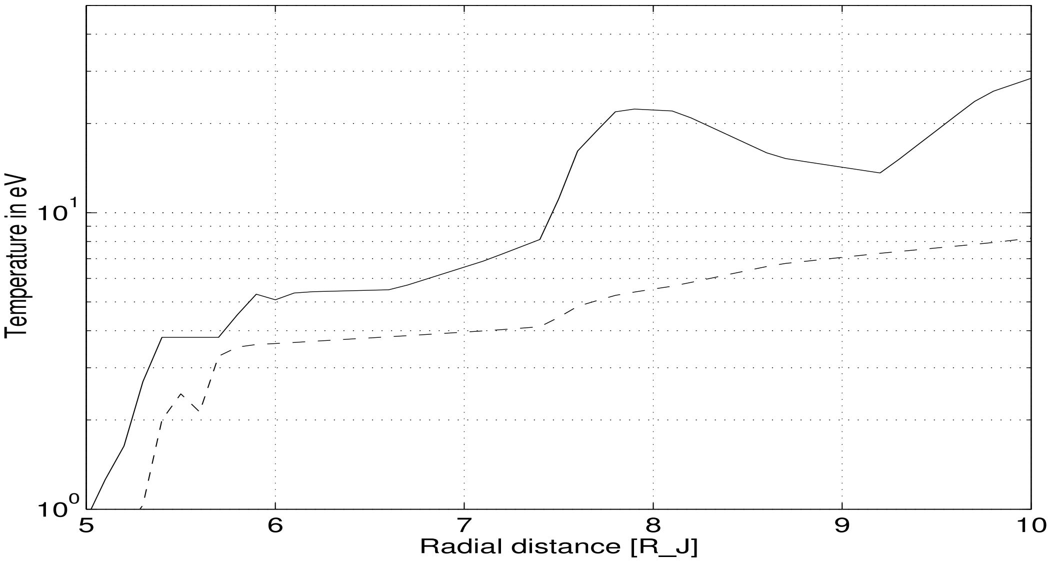

Figure 5. Electron temperature measured by the Voyager 1 spacecraft (solid line) compared with model calculated electron temperature (dashed line).

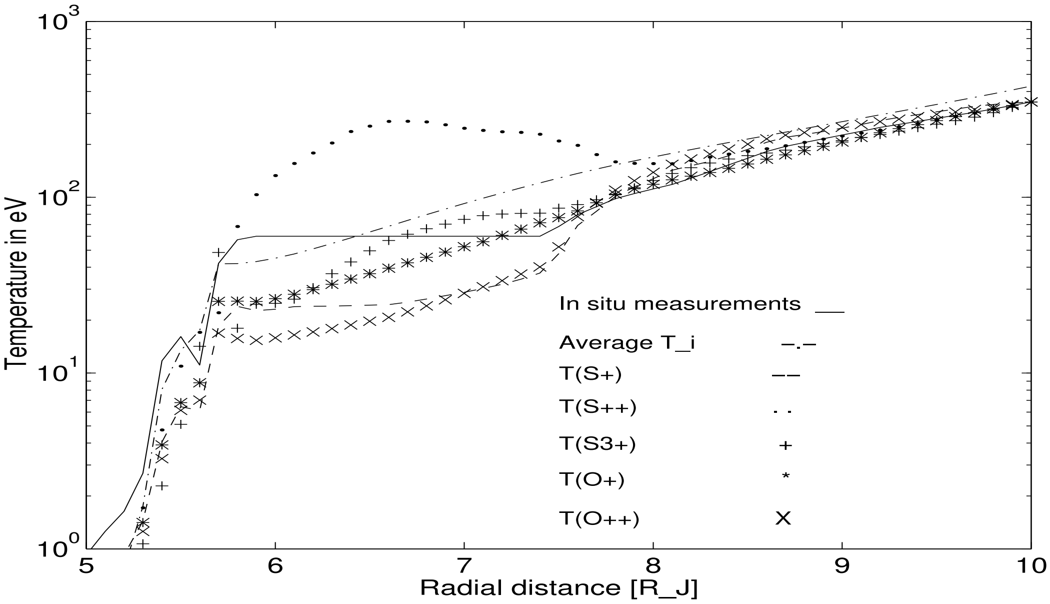

Figure 6. Computed temperatures of thermal ions, and mean temperature of all ion species compared with *in situ* temperature.

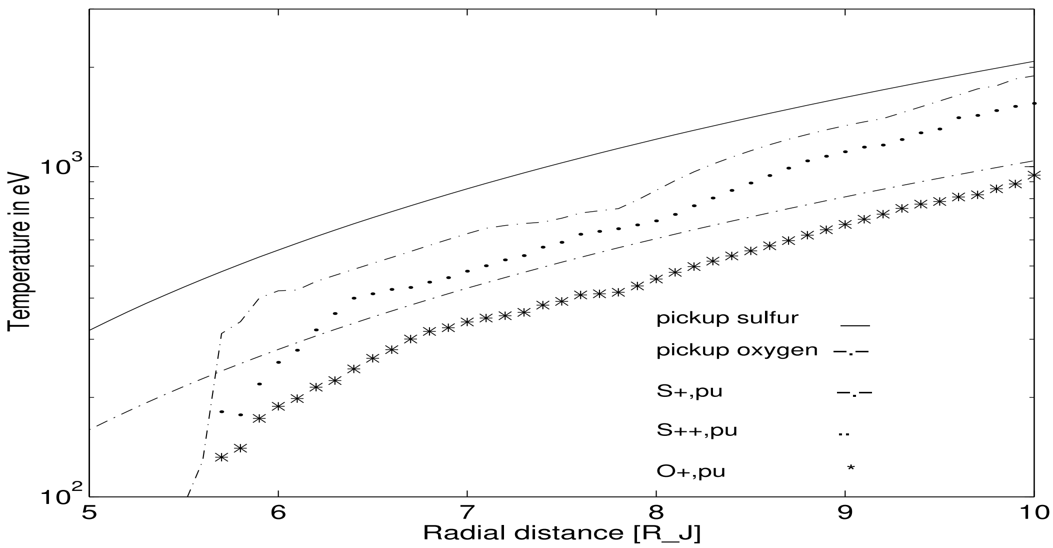

Figure 7. Calculated pickup ion temperatures compared with the energies of locally picked up ions.

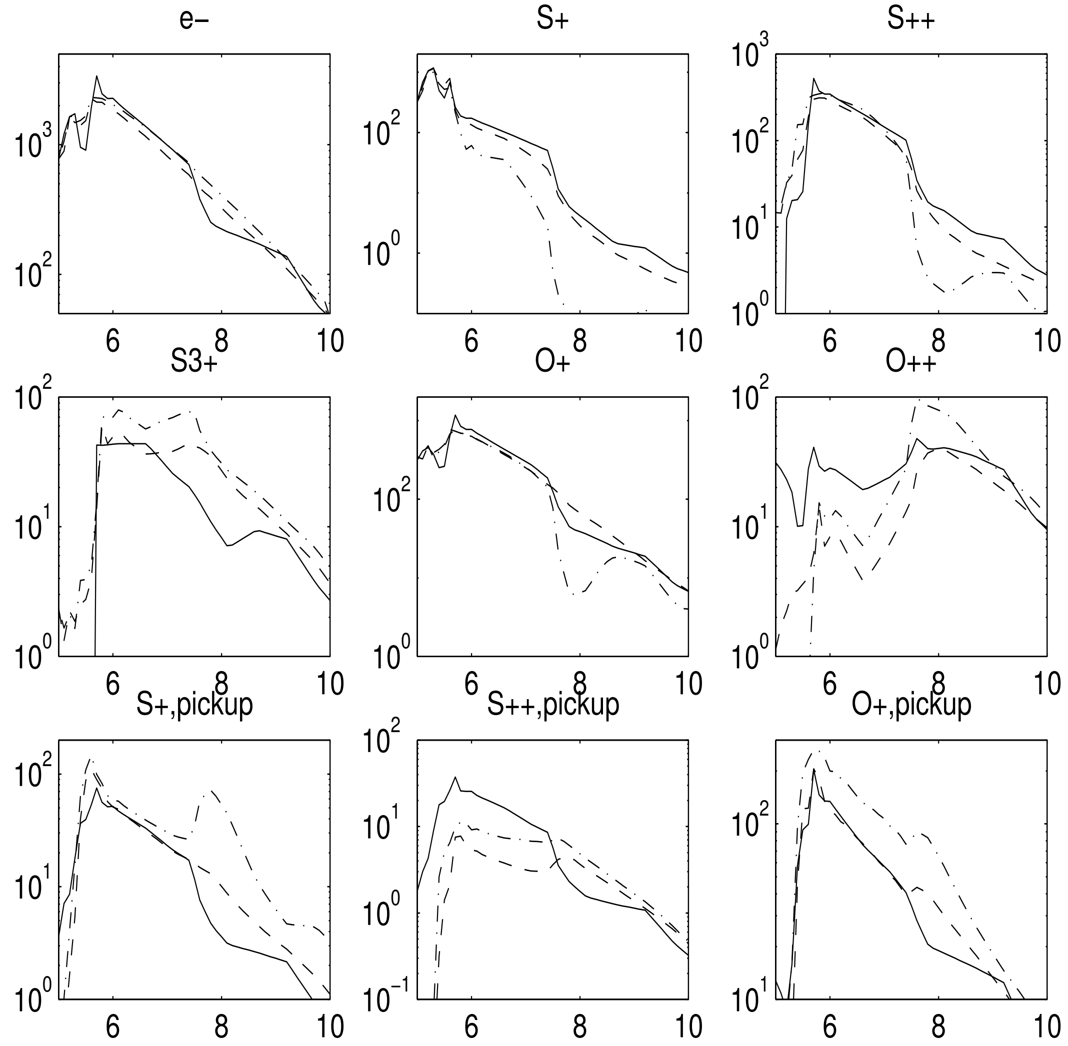

Figure 8. A comparison between various plasma species as given by the empirical model of *Bagenal* [1994] and the computed densities of various species using calculated T_e (dashed lines) and using the *in situ* measured T_e (dash-dotted lines).

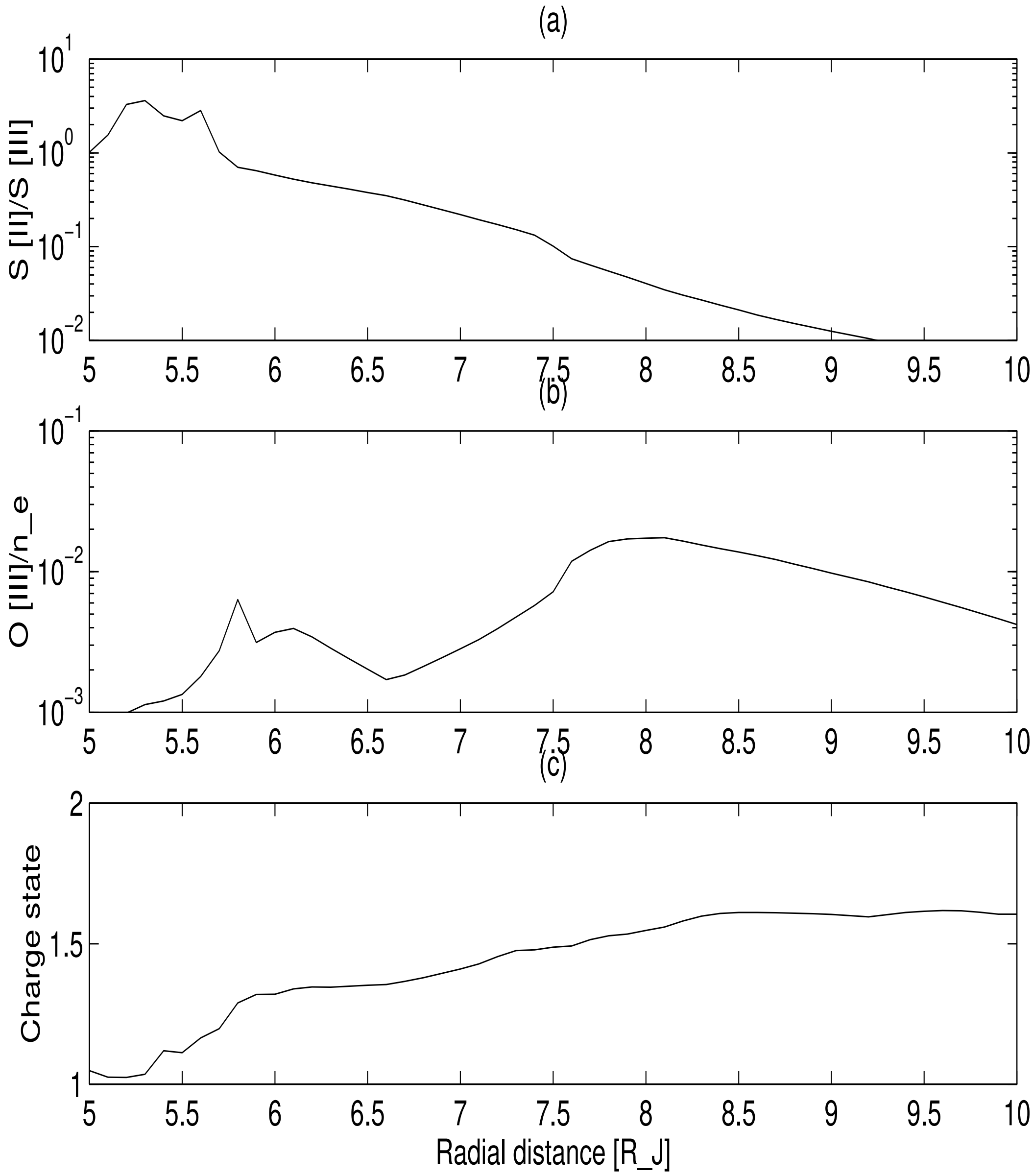

Figure 9. Radial profiles of the (a) $[S^{+}]/[S^{++}]$ ratio, (b) $[O^{++}]/n_e$ ratio, and (c) the ratio of ion density to electron density.

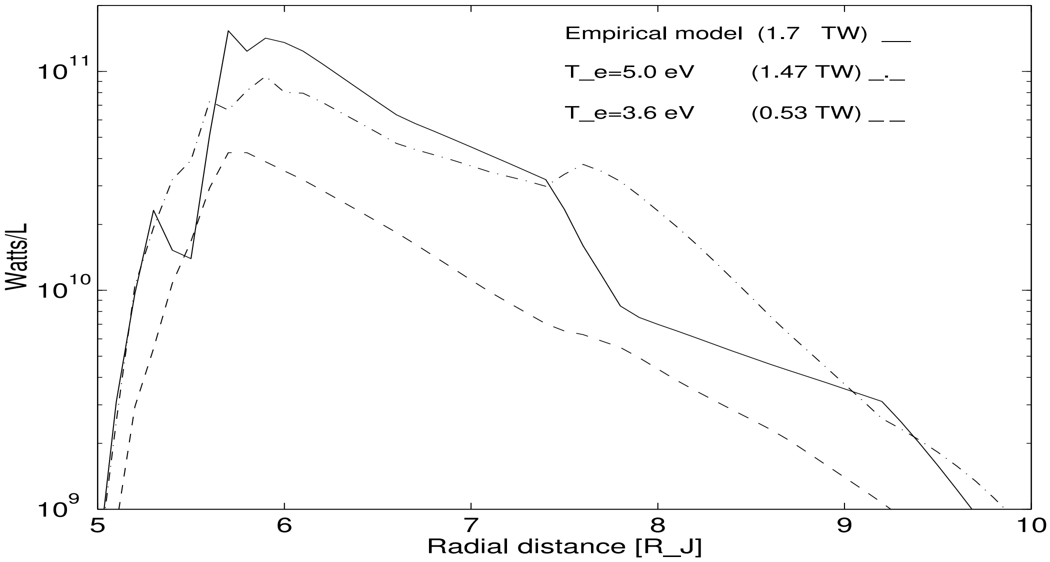

Figure 10. Profiles of the radiated emission. The solid line indicates the radiated emission using the empirical model ion and electron densities and temperatures. The dash-dotted line indicates radiated emission using the numerical model ion and electron densities but with electron temperatures left unchanged. The dashed line indicates radiated emission using the numerical model ion and electron densities and temperatures.

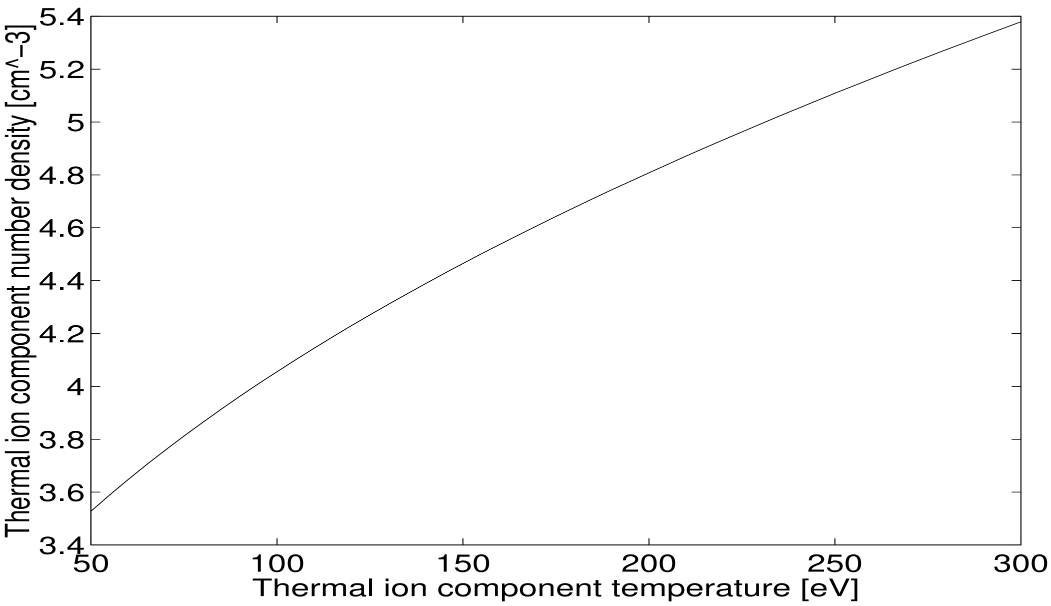

Figure 11. Number density of the thermal ion component required to raise the electron temperature from 3.6 to 5 eV, vs. the hot thermal component temperature.

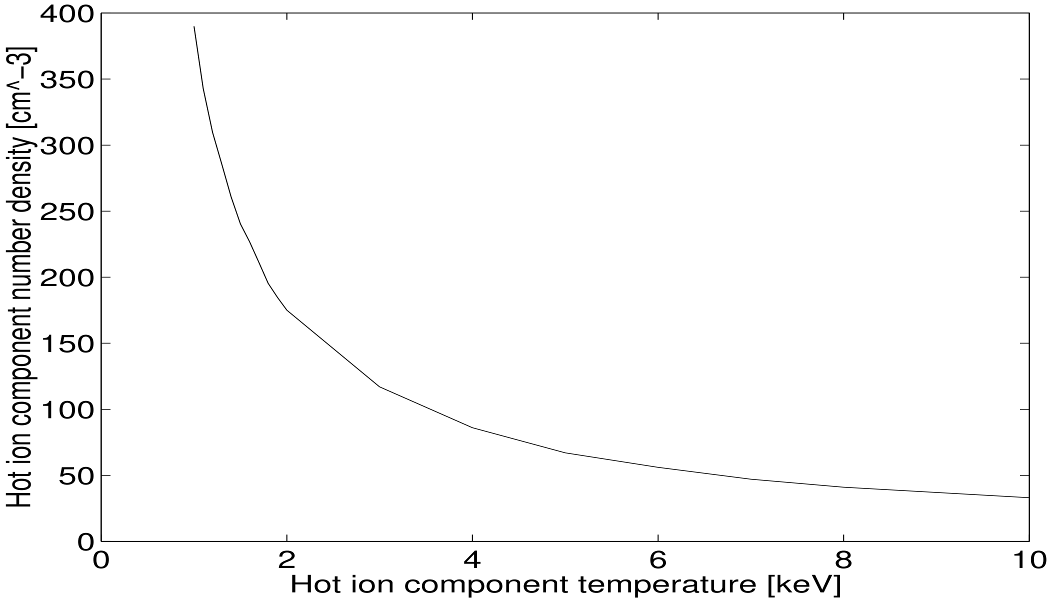

Figure 12. Number density of the hot ion component required to raise the electron temperature from 3.6 to 5 eV, vs. the hot ion component temperature.

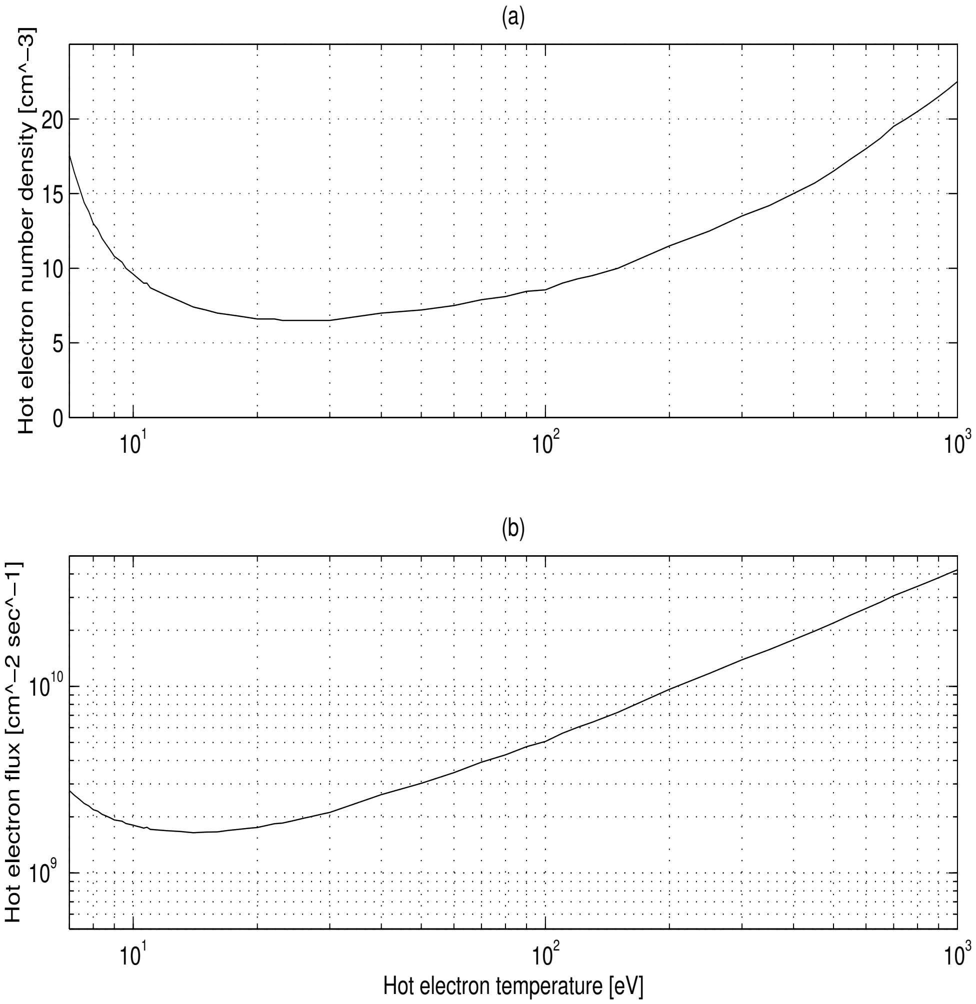

Figure 13. (a) Number density of the suprathermal electron component required to raise the electron temperature from 3.6 to 5 eV, vs. the suprathermal electron temperature. (b) Hot electron flux required for the above mentioned temperature raise.

Tables

Table 1. Diffusion coefficient in the cold and warm parts of the torus.

	Cold torus	Warm torus
K $[sec^{-1}]$	3.0×10^{-11}	3.6×10^{-10}
m	3	4

Table 2. Charge exchange reactions included in the model [*McGrath and Johnson*, 1989] and their rates at $L = 6$.

Charge exchange	
Reaction	κ $[\mathrm{cm}^3 \cdot \mathrm{sec}^{-1}]$
$S + S^+ \rightarrow S^+ + S$	$\kappa_1 = 2.4 \times 10^{-8}$
$S + S^{++} \rightarrow S^+ + S^+$	$\kappa_2 = 3 \times 10^{-10}$
$S + S^{++} \rightarrow S^{++} + S$	$\kappa_3 = 7.8 \times 10^{-9}$
$S + S^{3+} \rightarrow S^+ + S^{++}$	$\kappa_4 = 1.32 \times 10^{-8}$
$O + O^+ \rightarrow O^+ + O$	$\kappa_5 = 1.32 \times 10^{-8}$
$O + O^{++} \rightarrow O^+ + O^+$	$\kappa_6 = 5.2 \times 10^{-10}$
$O + O^{++} \rightarrow O^{++} + O$	$\kappa_7 = 5.4 \times 10^{-9}$
$O + S^+ \rightarrow O^+ + S$	$\kappa_8 = 9 \times 10^{-11}$
$S + O^+ \rightarrow S^+ + O$	$\kappa_9 = 3 \times 10^{-9}$
$S + O^{++} \rightarrow S^+ + O^+$	$\kappa_{10} = 2.34 \times 10^{-8}$
$S + O^{++} \rightarrow S^{++} + O^+ + e^-$	$\kappa_{11} = 1.62 \times 10^{-8}$
$O + S^{++} \rightarrow O^+ + S^+$	$\kappa_{12} = 2.3 \times 10^{-9}$
$O^{++} + S^+ \rightarrow O^+ + S^{++}$	$\kappa_{13} = 1.4 \times 10^{-9}$
$O + S^{3+} \rightarrow O^+ + S^{++}$	$\kappa_{14} = 1.92 \times 10^{-8}$
$O^{++} + S^{++} \rightarrow O^+ + S^{3+}$	$\kappa_{15} = 9 \times 10^{-9}$

Table 3. Diffusion time in the warm torus.

L_{out}	D_{LL} [s^{-1}]	$\int_{L_{in}}^{L_{out}} N\,dL$	$dY/dL\,\|_{L_{out}}$	τ_D [Days]
7.0	8.6×10^{-7}	5.3×10^{34}	-5.6×10^{35}	63
7.5	1.1×10^{-6}	6.5×10^{34}	-4.4×10^{35}	84
8.0	1.5×10^{-6}	7.3×10^{34}	-4.2×10^{35}	86.5

Table 4. Radiative emission lines

Ion	wavelength [$\AA$]	Transition (i,j)	Ω(j,i)
S II	6724	2,1	5.7
S II	4069	3,1	2.7
S II	1256	4,1	6.7
S II	910	7,1	2.3
S II	765		7.1
S III	9532	2,1	3.87
S III	6312	3,2	1.34
S III	3722	3,1	0.75
S III	1729	4,1	2.3
S III	1198	5,1	4.0
S III	1018	6,1	3.0
S III	825	12,3	0.5
S III	685	12,1	55.9
S IV	1406	2,1	4.5
S IV	1073	3,1	8.2
S IV	816	4,1	1.0
S IV	750	5,1	6.8
S IV	661	6,1	9.8
O II	3727	2,1	1.47
O II	2471	3,1	0.5
O II	834	4,1	4.1
O II	539	6,1	0.5
O III	5007	2,1	2.5
O III	4363	3,2	0.58
O III	1664		5.0
O III	835	5,1	7.4
O III	703	6,1	5.8
O III	508	8,1	2.8

Figures

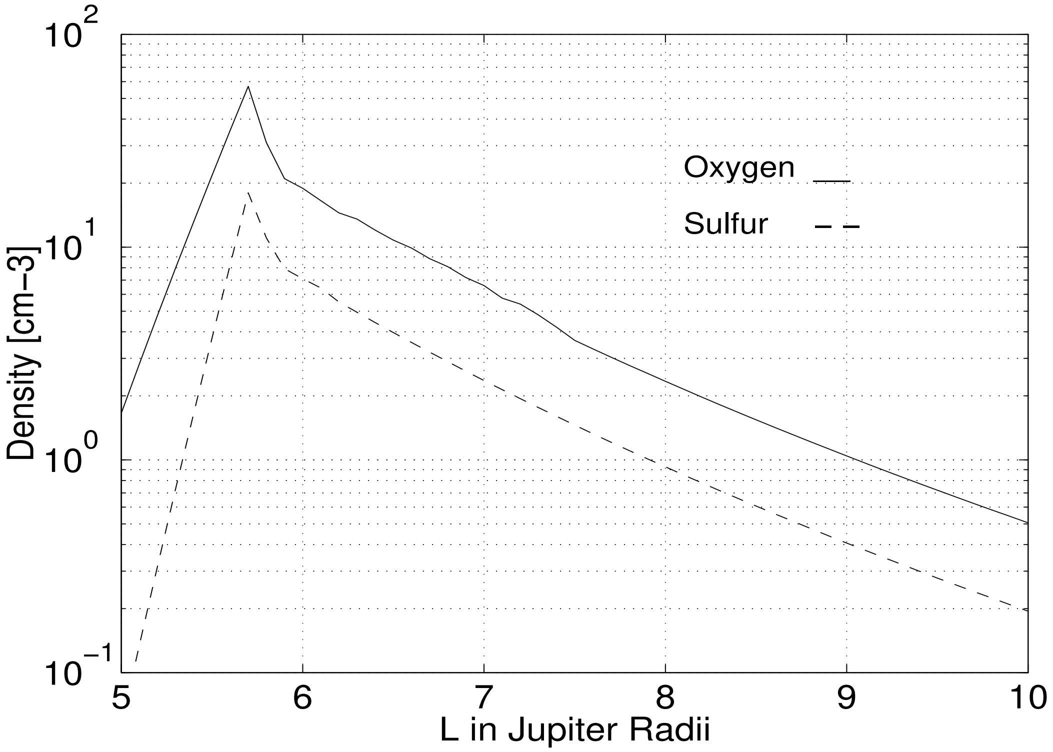

Figure 1. Density profile of neutral oxygen and sulfur along the equator.

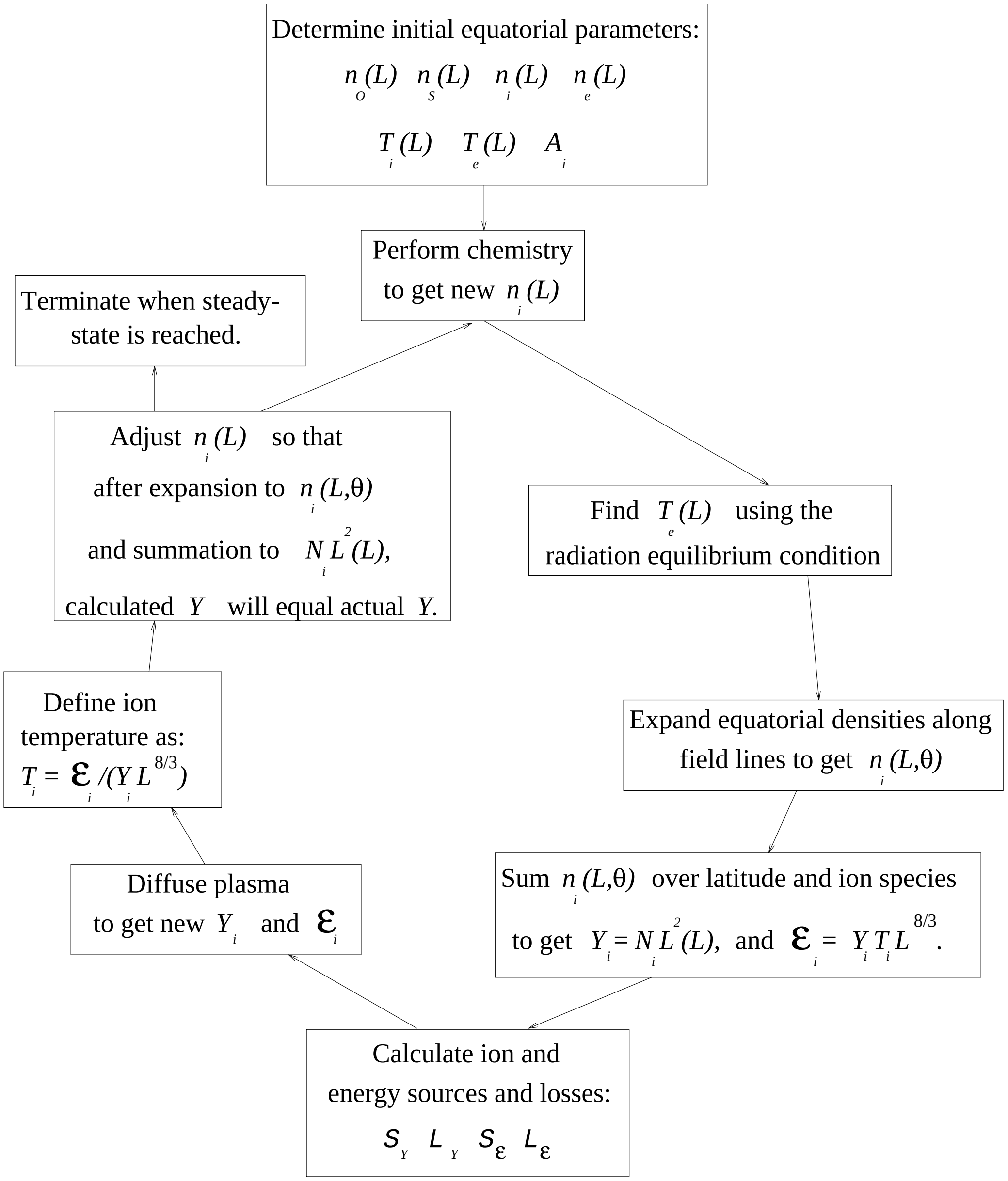

Figure 2. Schematic diagram showing a flow chart of the model calculations used.

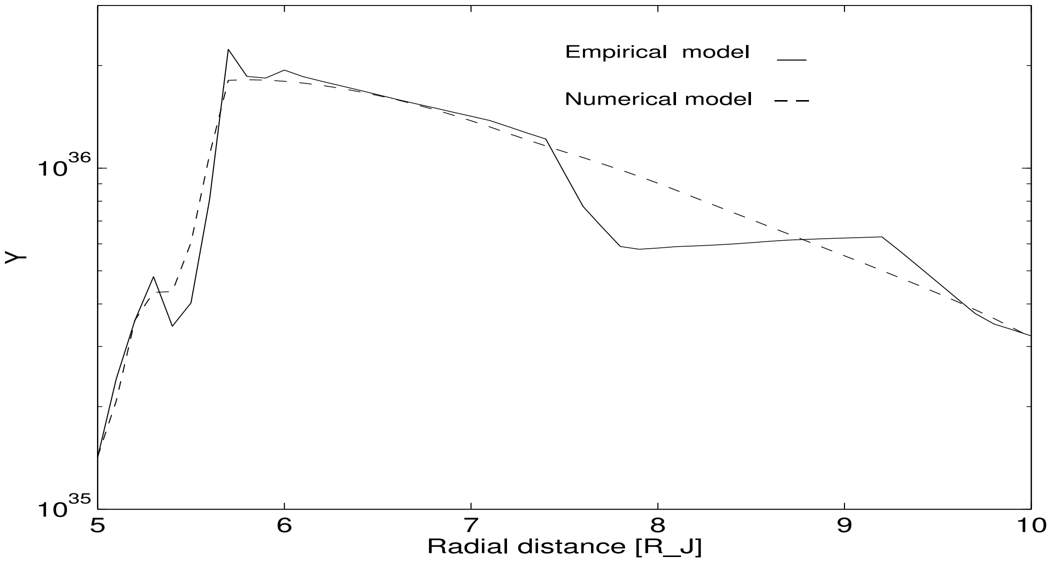

Figure 3. A comparison between the flux tube content profile as given by the empirical model of *Bagenal* [1994] (solid line), and the numerical model (dashed line).

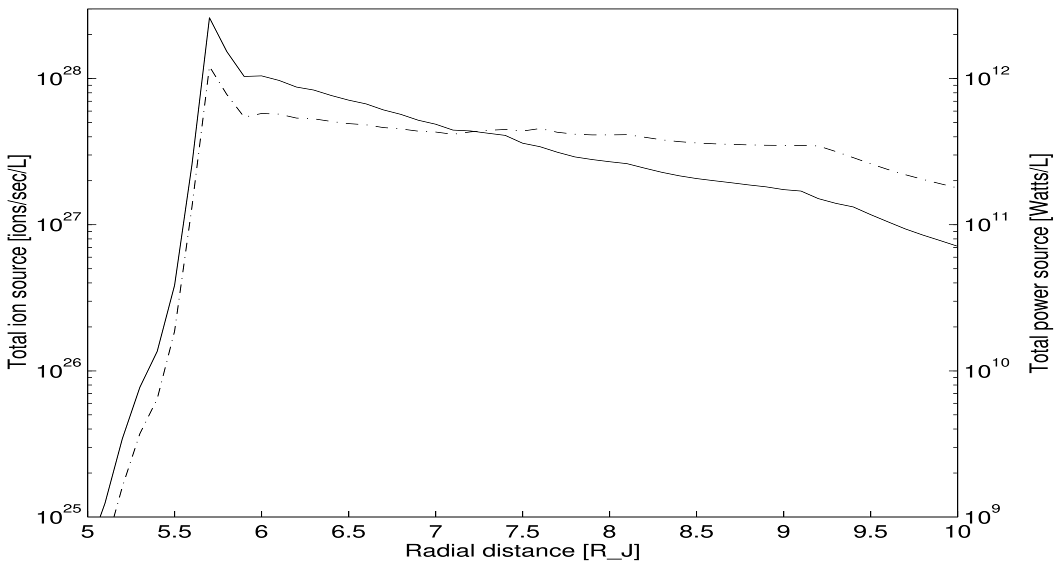

Figure 4. Total ion source rate in ions per sec per unit L (solid line), and total power source in W per unit L (dashed line).

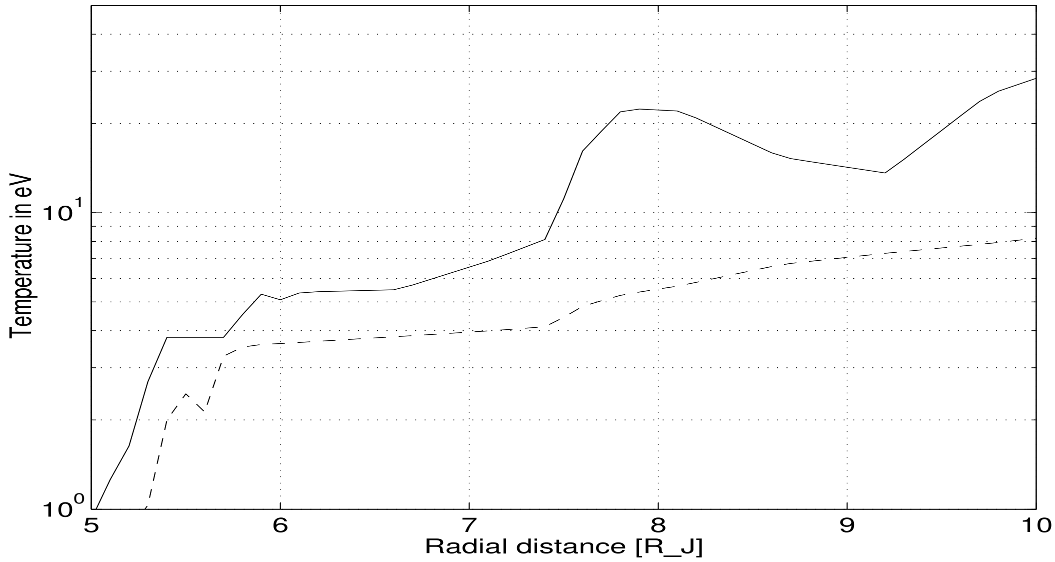

Figure 5. Electron temperature measured by the Voyager 1 spacecraft (solid line) compared with model calculated electron temperature (dashed line).

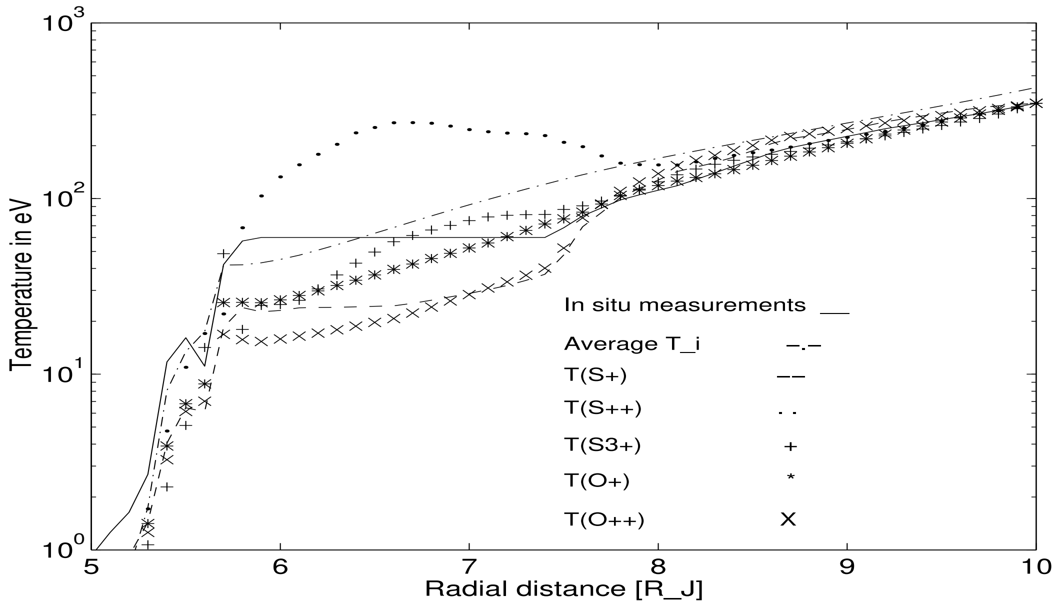

Figure 6. Computed temperatures of thermal ions, and mean temperature of all ion species compared with *in situ* temperature.

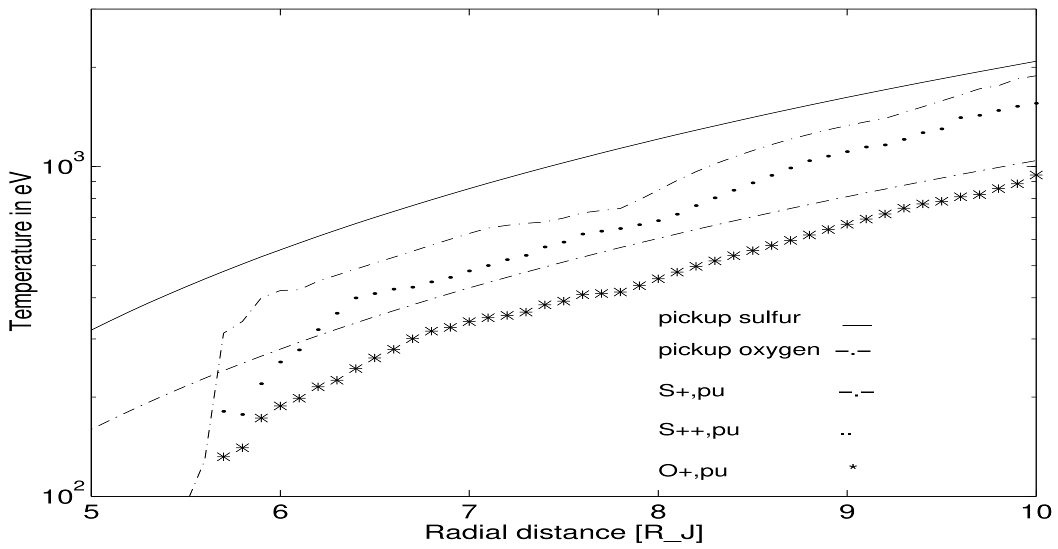

Figure 7. Calculated pickup ion temperatures compared with the energies of locally picked up ions.

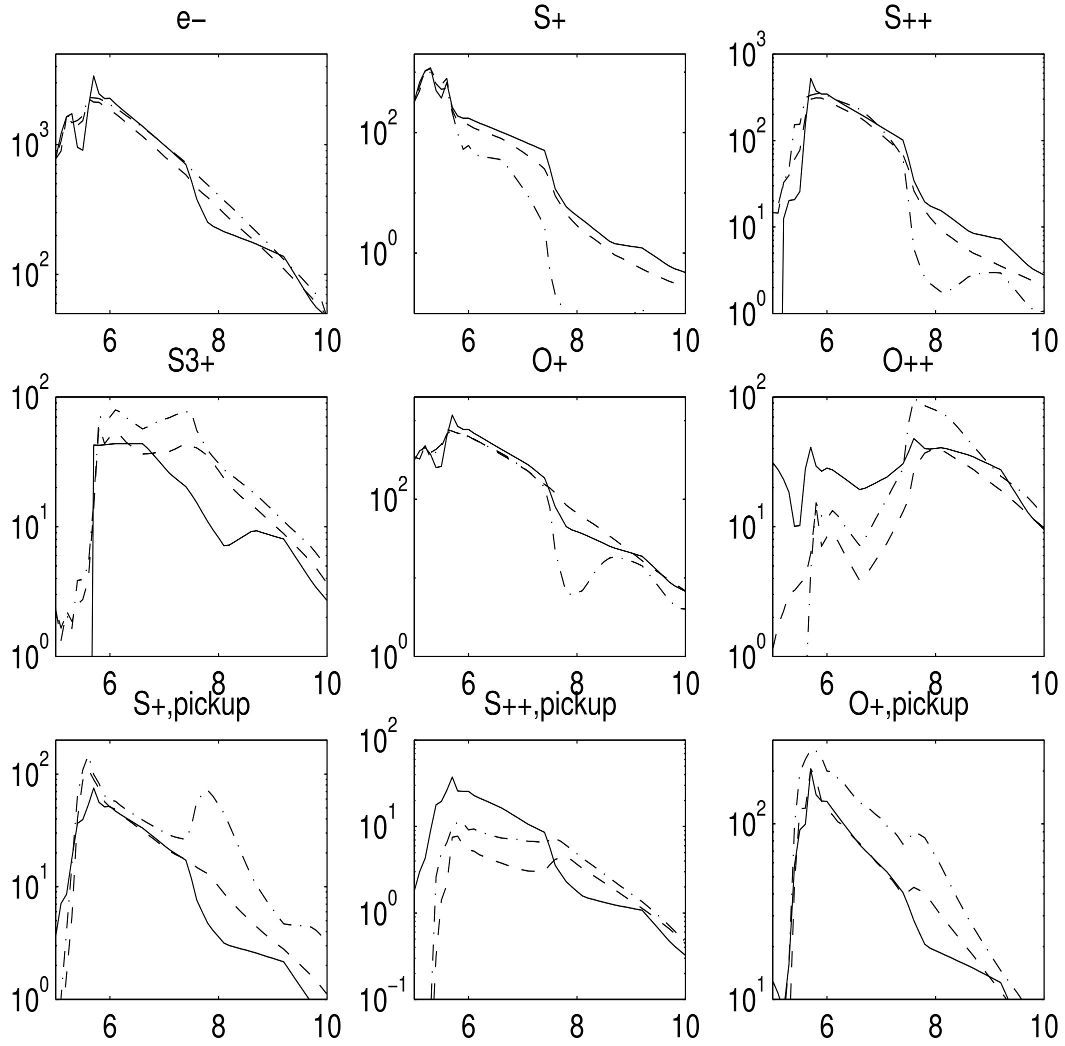

Figure 8. A comparison between various plasma species as given by the empirical model of *Bagenal* [1994] and the computed densities of various species using calculated T_e (dashed lines) and using the *in situ* measured T_e (dash-dotted lines).

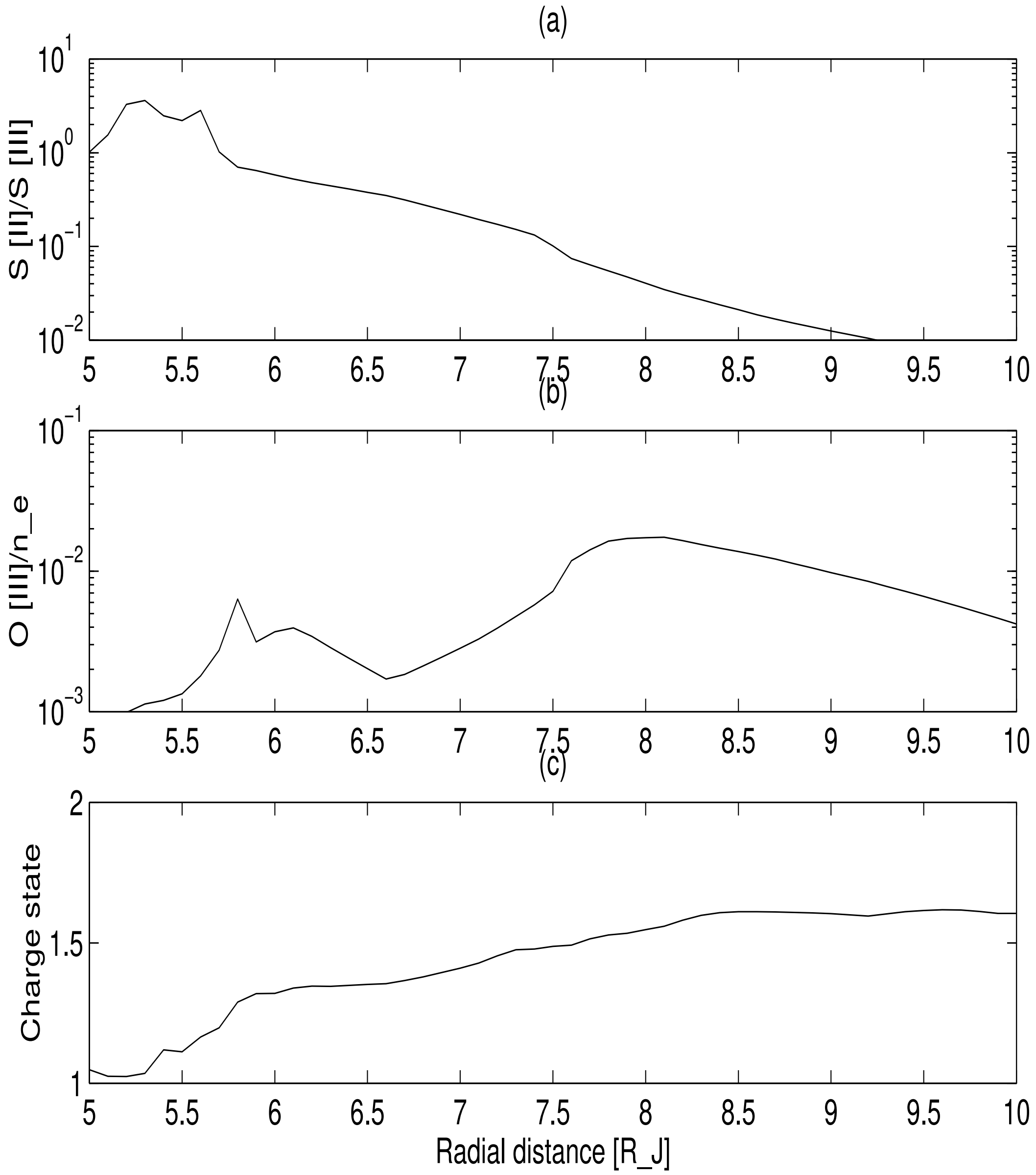

Figure 9. Radial profiles of the (a) $[S^{+}]/[S^{++}]$ ratio, (b) $[O^{++}]/n_e$ ratio, and (c) the ratio of ion density to electron density.

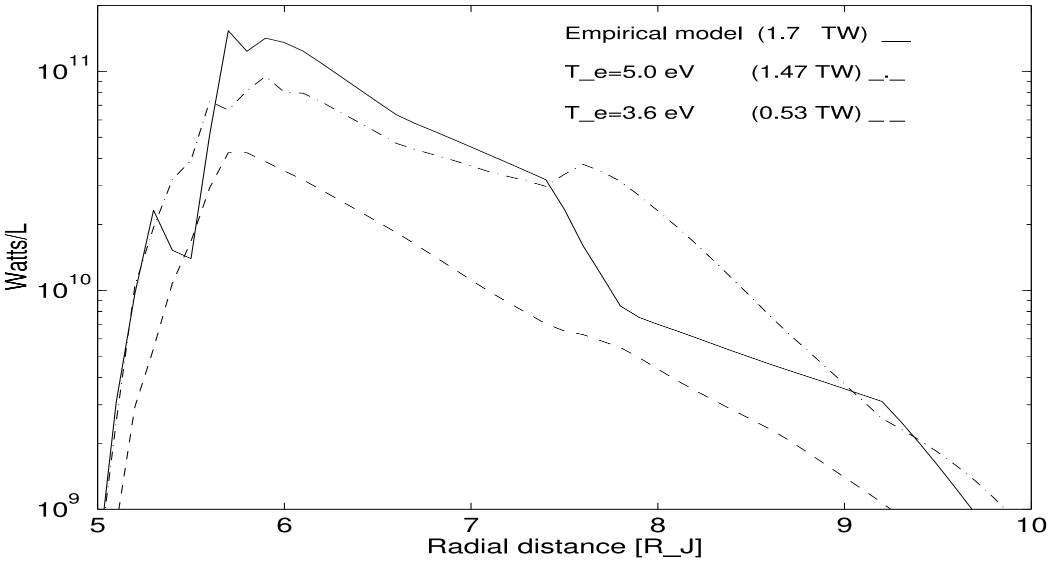

Figure 10. Profiles of the radiated emission. The solid line indicates the radiated emission using the empirical model ion and electron densities and temperatures. The dash-dotted line indicates radiated emission using the numerical model ion and electron densities but with electron temperatures left unchanged. The dashed line indicates radiated emission using the numerical model ion and electron densities and temperatures.

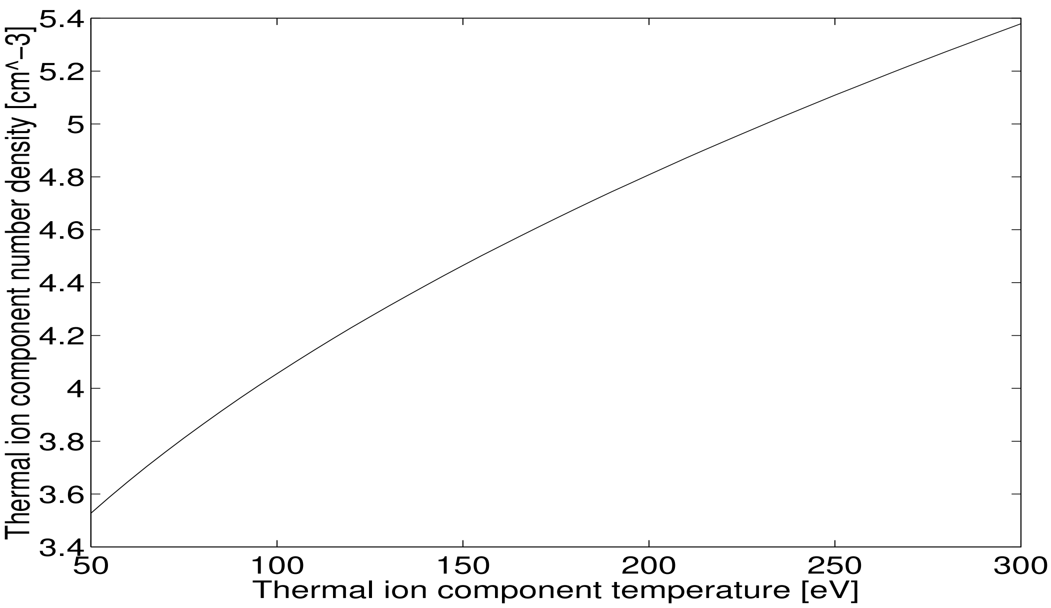

Figure 11. Number density of the thermal ion component required to raise the electron temperature from 3.6 to 5 eV, vs. the hot thermal component temperature.

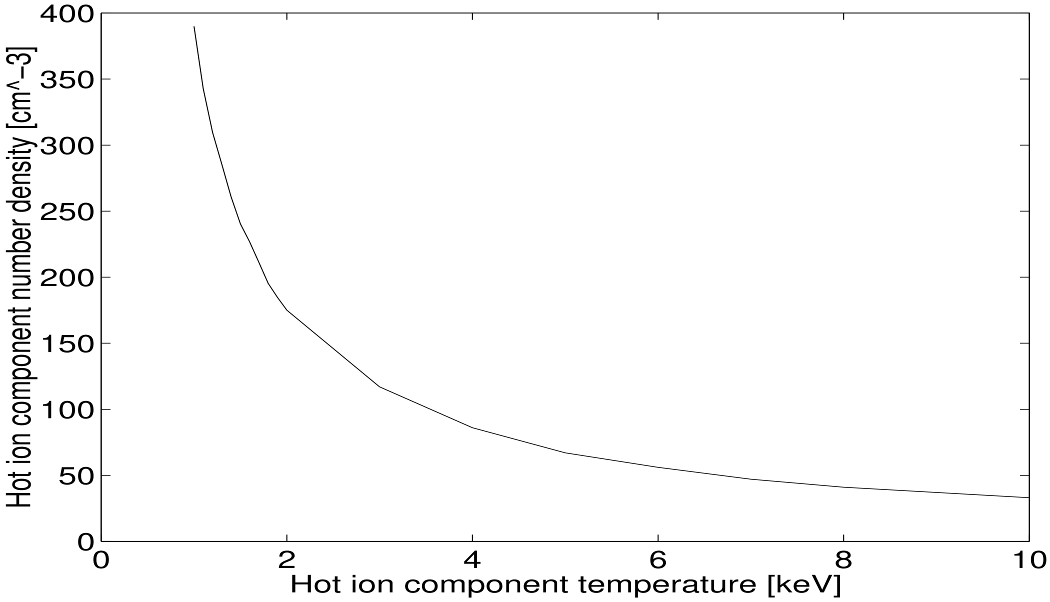

Figure 12. Number density of the hot ion component required to raise the electron temperature from 3.6 to 5 eV, vs. the hot ion component temperature.

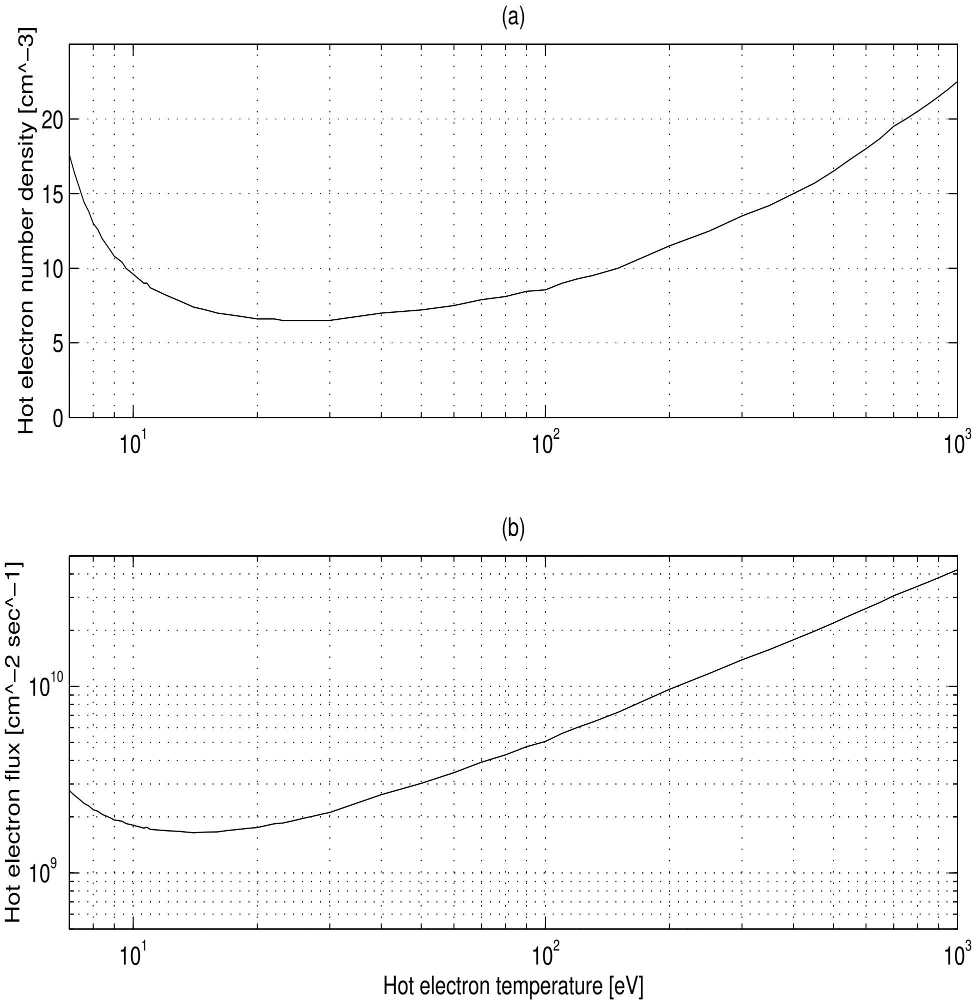

Figure 13. (a) Number density of the suprathermal electron component required to raise the electron temperature from 3.6 to 5 eV, vs. the suprathermal electron temperature. (b) Hot electron flux required for the above mentioned temperature raise.